NASA TECHNICAL NOTE

NASA TN D-4907

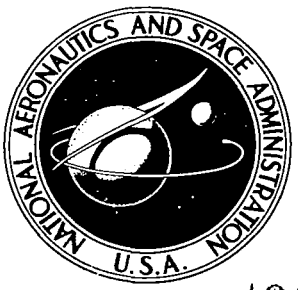

NASA TN D-4907

HEAT-TRANSFER AND PRESSURE DISTRIBUTIONS DUE TO SINUSOIDAL DISTORTIONS ON A FLAT PLATE AT MACH 20 IN HELIUM

by James P. Arrington

Langley Research Center
Langley Station, Hampton, Va.

NATIONAL AERONAUTICS AND SPACE ADMINISTRATION • WASHINGTON, D. C. • NOVEMBER 1968

HEAT-TRANSFER AND PRESSURE DISTRIBUTIONS DUE TO SINUSOIDAL DISTORTIONS ON A FLAT PLATE AT MACH 20 IN HELIUM

By James P. Arrington

Langley Research Center
Langley Station, Hampton, Va.

NATIONAL AERONAUTICS AND SPACE ADMINISTRATION

For sale by the Clearinghouse for Federal Scientific and Technical Information
Springfield, Virginia 22151 – CFSTI price $3.00

HEAT-TRANSFER AND PRESSURE DISTRIBUTIONS DUE TO SINUSOIDAL DISTORTIONS ON A FLAT PLATE AT MACH 20 IN HELIUM*

By James P. Arrington
Langley Research Center

SUMMARY

An experimental investigation was conducted to determine the effects of a two-dimensional repetitive sine-wave distortion on the pressure and heat-transfer distributions. Tests were made on a sharp flat plate with a distorted section in a relatively thick boundary layer which changed from laminar to transitional for certain test conditions. The tests were conducted in helium at free-stream Mach numbers of about 20, over a range of length Reynolds numbers varying from 2.72×10^6 to 8.80×10^6 with the flat-plate surface at angles of inclination of 0°, 5°, and 10°.

The results of the present tests were similar to results obtained in air at lower free-stream Mach numbers and Reynolds numbers with relatively thinner boundary layers. The pressure and heat-transfer distributions were greatly altered in the distorted section (oscillating from maximum to minimum values) with the heating distribution being affected the most. The magnitude of these pressure and heat-transfer oscillations also depended on whether the flow was laminar or transitional. However, the values generally approached the undisturbed flat-plate results a short distance downstream of the distorted region.

The Savage-Nagel attached laminar-flow theory for shallow waves adequately predicted the first-wave maximum pressures for attached laminar flow. However, the theory was not routinely successful in predicting the first-wave maximum pressures in separated flow and the first-wave maximum heat-transfer results for attached and separated laminar flow. For different angles of attack, the first-wave maximum laminar heating was correlated with results obtained in air in a previous Mach 10 investigation.

---

*The information presented herein is largely based on a thesis entitled "Heat Transfer and Pressure Distributions in Regions of Sinusoidal Protuberances on a Flat Plate," submitted in partial fulfillment of the requirements for the degree of Master of Science in Aerospace Engineering, Virginia Polytechnic Institute, Blacksburg, Virginia, 1966.

INTRODUCTION

Surface irregularities can be expected to exist on full-scale vehicles because of manufacturing methods, load deformations, and/or thermal conditions. Since the design and the choice of material and structural surfaces are dictated by the severe heating associated with hypersonic flight, a knowledge of surface distortion effects on local heating rates is desirable.

Although a great deal of work has been reported for single steps, wedges, and smooth protuberances (see, for example, refs. 1 to 5), only a relatively few studies concerning repetitive protuberances have been published. Rhudy and Magnan (ref. 6) presented experimental laminar and turbulent results for swept and unswept surface distortions in relatively thin boundary layers at a free-stream Mach number of 10. Jaeck in reference 7 compared the maximum pressure and heating results of Rhudy and Magnan with a Savage-Nagel shallow-wave theory. However, Bertram and his coworkers (ref. 8) found that this theory was inadequate when correlating a portion of the results from the present investigation and those of reference 9. For these cases the maximum heating on a repetitive sine wave in laminar flow was represented by an empirical relationship.

The present tests provide a detailed study of relatively thick laminar and transitional boundary-layer flow over a flat plate with sharp leading edge and an unswept repetitive sine-wave distorted section, at free-stream Mach numbers of about 20. The length Reynolds number ranged from 2.72×10^6 to 8.80×10^6 and the angles of inclination were 0^o, 5^o, and 10^o. The investigation is supported by schlieren and oil-flow studies, a flow-field survey, pressure distributions, and heat-transfer distributions. The heat-transfer and pressure distributions, including the maximum pressures and heating on the distorted section, are compared with theoretical predictions, and where possible the data are compared with previously published results.

SYMBOLS

Measurements for this investigation were taken in the U.S. Customary System of Units. Equivalent values in the International System (SI) were obtained by using conversion factors given in reference 10 and are indicated parenthetically.

C' Chapman-Rubesin constant, $\frac{\mu' T_\infty}{\mu_\infty T'}$

c specific heat, Btu/lb-^{o}R (joules/kilogram-^{o}K)

c_p specific heat at constant pressure, Btu/lb-^{o}R (joules/kilogram-^{o}K)

$$G = 1.7208 \frac{\gamma - 1}{2}\left(\frac{T_w}{T_r} + \frac{4.65N_{Pr}^{1/3} - 3.65N_{Pr}^{1/2}}{2.59} N_{Pr}^{1/2}\right)$$

H	maximum height of sine wave above flat plate, in. (centimeters)
h	film coefficient of heat transfer, $\frac{\dot{q}}{T_{aw} - T_w}$
k	thermal conductivity, Btu/ft-sec-^{o}R (joules/meter-second-^{o}K)
L	model reference length, in. (centimeters)
M	Mach number
N_{Pr}	Prandtl number, $\frac{c_p \mu}{k}$
N_{St}	Stanton number, $\frac{h}{c_{p,\infty}\rho_\infty V_\infty}$
p	pressure, psi (newtons/meter^2)
$p_{t,2}$	total pressure behind a normal shock, psi (newtons/meter^2)
$\dot{q}$	surface heat-transfer rate, Btu/ft^2-sec (joules/meter^2-second)
R	Reynolds number (subscripts indicate reference conditions)
s	distance from leading edge to beginning of first sine wave, in. (centimeters)
T	temperature, ^{o}R (^{o}K)
T'	reference static temperature, ^{o}R (^{o}K)
t	time, second
V	velocity, ft/sec (meters/second)
x	distance parallel to flat part of surface, measured from leading edge, in. (centimeters)

y	distance measured normal from flat part of model surface, in. (centimeters)
y_s	distance measured normal from flat part of model surface to leading-edge shock (from schlieren photographs), in. (centimeters)
α	angle of inclination, degrees
γ	ratio of specific heats
δ	boundary-layer thickness, in. (centimeters)
δ^*	boundary-layer displacement thickness, in. (centimeters)
η	recovery factor, $\frac{T_{aw} - T_\infty}{T_t - T_\infty}$
λ_∞	viscous interaction parameter, $\frac{G}{2}\frac{M_\infty^3\sqrt{C'}}{R_{\infty,x}}$
μ	coefficient of viscosity, lb/ft-sec (kilograms/meter-second)
μ'	coefficient of viscosity based on T', lb/ft-sec (kilograms/meter-second)
ρ	density, lb/ft^3 ($kilograms/meter^3$)
τ	skin thickness, ft (meters)

Subscripts:

aw	adiabatic wall
d	leading-edge thickness
f_p	flat plate
i	inviscid
L	model reference length, in. (centimeters)
l	local flat-plate conditions

m	pertaining to model
max	maximum
min	minimum
r	recovery
t	stagnation
w	wall
x	distance measured parallel to model flat surfaces, in. (centimeters)
σ	beginning of flow separation
∞	free stream

APPARATUS AND TESTS

Wind Tunnel

This investigation was conducted in the Langley 22-inch helium tunnel. (See fig. 1.) The tunnel (described in ref. 11) is a closed-cycle, intermittent, blowdown facility.

To conduct tests over a range of free-stream unit Reynolds numbers, the tunnel must be operated over a large range of stagnation pressures. These changes in stagnation pressure result in changes in the tunnel-wall boundary layer which alter the effective expansion of the nozzle. The contoured nozzle with a throat diameter of 0.622 inch (1.58 cm) was previously calibrated for various stagnation pressures at room temperature (approximately 535° R or 297° K) and the results are presented in reference 11. Calibration checks were made during the present tests, and the Mach number was found to be independent of stagnation temperature – at least up to 860° R (478° K). A summary of the Mach number calibration is presented in figure 2 as a function of stagnation pressure.

Models

A photograph of the configuration studied in this investigation is presented in figure 3. The model was a 10° wedge with a 0.003-inch (0.0076-cm) leading-edge thickness. It had a section of successive unswept sine waves on one surface and a flat plate on the

other surface. Three models were constructed in order to obtain data on pressure distributions, heat-transfer rates, and schlieren and oil-flow patterns. Swept end plates were attached to the pressure, heat-transfer, and oil-flow models.

The 0.030-inch (0.076-cm) inconel skin of the heat-transfer model was attached to both sides of a support frame; this allowed the thermocouple wires to be routed inside the hollow model. The thermocouples were spotwelded to the inner side of the skin along several longitudinal rows as shown in figure 4 and listed in table I. The instrumentation was brought out of the tunnel through a side-mounted strut which was attached to a window blank. (See fig. 3.)

The construction of the pressure model was similar to that of the heat-transfer model except that the skin thickness was increased to 0.060 inch (0.152 cm). The pressure orifices were formed from 0.060-inch (0.152-cm) inside-diameter tubing which was connected to 0.090-inch (0.229-cm) inside-diameter tubing outside of the model. The orifices were alined along rows as shown in figure 4 and table II.

A fiber-glass model was constructed for oil-flow and schlieren studies. This model was sting-supported from the base since utilization of the test-section windows was necessary.

In addition to surface-pressure measurements, impact-pressure measurements were made from the model surface out to the undisturbed free stream. The pitot-pressure survey rake used for this study consisted of three tubes fastened to a bracket as shown in figure 5. This bracket could be raised and lowered by an attachment at the base of the test model.

Instrumentation

The stagnation pressures were read from a Bourbon tube gage, and the stagnation temperature was obtained from both an iron-constantan thermocouple in the stagnation chamber and an iron-constantan total-temperature probe in the test section. The heat-transfer model was also instrumented with iron-constantan thermocouples. The model surface pressures were measured by means of ionization gages employing a radioactive source to ionize the sampled gas. These gages operate in two ranges, 0 to 30 mm Hg and 0 to 3 mm Hg. Above 1 mm Hg the gages are accurate to ±5 percent of the reading.

Impact pressures were measured by means of diaphragm-type transducers. This instrument has an accuracy of ±0.25 percent of the full-scale values. In order to maintain maximum accuracy of measurements, gages of four different ranges were used: 1, 3, 5, and 7.5 psia (6.89, 20.7, 34.5, and 51.7 kilonewtons/meter^2).

Test Conditions and Procedures

The tests were conducted at a stagnation temperature of 860° R (478° K) and at stagnation pressures of 750, 2000, and 3000 psig (5.2, 13.8, and 20.7 meganewtons/meter^2). These conditions provided test Mach numbers of 19.8, 21.6, and 22.2, respectively, and unit Reynolds numbers of 0.17×10^6, 0.40×10^6, and 0.55×10^6 per inch (0.067×10^6, 0.157×10^6, and 0.216×10^6 per cm), respectively.

Prior to testing the pressure models, the tubing and ionization gages were purged with helium until the gages correctly read the pressure in the evacuated tunnel. The outputs of the gages were recorded at approximately 2-second intervals throughout the tests, which were terminated after the readings had settled to constant values. By using a variable diffuser, an operating time of approximately 1 minute was possible.

Before testing the heat-transfer model, the stagnation chamber was initially pressurized with a plug in the throat of the nozzle. The plug was rapidly withdrawn to obtain a quick start, and a hydraulically operated pressure-control valve automatically maintained the proper stagnation pressure for the duration of the run (approximately 6 seconds).

The technique for obtaining surface oil-flow patterns consisted of first applying a thin coat of silicone oil and then using a hypodermic needle to place small dots of a mixture of oil and lampblack over the surface of the fiber-glass model. This model was rolled 90° in the tunnel. While the tests were in progress photographs were taken (through the test-section windows) with a camera positioned approximately normal to the surface being photographed. After the picture was taken and while the test was still in progress, the position of the oil line indicating the region of separation ahead of the first wave was obtained by locating the center of the separation line with a coordinate cathetometer.

Reduction of Heat-Transfer Data

The local heating rate was computed from the thin-skin equation,

$$\dot{q} = c_m \rho_m \tau_m \frac{dT_w}{dt} \tag{1}$$

where the rate of surface temperature rise was obtained from a card-programed computer which fitted a second-degree curve by the method of least squares to the temperature-time data (20 points per second). The curve fit to the data was applied about 1 second after the start of the test; this was approximately the time required for flow conditions to be established in the nozzle (using the quick-starting technique). This

quick-starting technique is an approximation for a step function applied to the heat-transfer coefficient. The properties of inconel given in reference 12 were used in evaluating the heat-transfer data.

Conduction corrections were calculated and found to be negligible; hence, the measured local heat-transfer coefficient was calculated from the relation

$$h = \frac{\dot{q}}{T_{aw} - T_w} \tag{2}$$

The adiabatic-wall temperature was obtained from the equation

$$\frac{T_{aw}}{T_t} = \eta + (1 - \eta)\left(\frac{p_l}{p_{t,l}}\right)^{\frac{\gamma-1}{\gamma}} \tag{3}$$

The recovery factor η was assumed to be the square root of the Prandtl number (a Prandtl number of 0.688 for helium was taken from the curves of Nicoll in ref. 13). For zero angle of inclination the local total pressure was not known. It was assumed to have a value between the total pressure behind a normal shock and the total pressure behind an oblique shock whose strength would produce the measured ratio of local static pressure to free-stream static pressure.

The values of T_{aw} corresponding to these two local total pressures are shown in figure 6 for a range of p_w/p_∞. For $\alpha = 0^\circ$, the average between the two T_{aw} curves was used in equation (2). For $\alpha = 5^\circ$ and 10°, the local total pressure was obtained from oblique-shock tables (ref. 14), and T_{aw} was calculated from equation (3).

RESULTS AND DISCUSSION

Flow Visualization

Schlieren studies.- Schlieren studies were made in order to determine the relative height of the wavy surface with respect to the boundary-layer thickness, to examine the separation and reattachment ahead of and within the wavy section, and to observe the shock system. Schlieren photographs of the fiber-glass model with the end plates removed are shown in figures 7, 8, and 9, for three angles of inclination and three different unit Reynolds numbers.

The apparent thickness of the laminar boundary layer relative to the height of the waves is shown for $\alpha = 0^\circ$ in figure 7. The first and last waves protruded out to about a third and a fifth of the boundary-layer thickness, respectively. At $\alpha = 5^\circ$ and 10°, the heights of the waves were about a half, and about equal to, the height of the boundary layer, respectively.

Surface oil-flow studies.- Surface oil-flow studies were incorporated into the test program in order to determine the effects of the end plates on the two-dimensionality of the model boundary layer, to determine the extent of the separation region, and to observe how separation is affected by changes in angle of inclination (local Mach number) and unit Reynolds number. Surface oil-flow patterns on the white fiber-glass model with end plates attached are presented in figures 10, 11, and 12, for three angles of inclination at three unit Reynolds numbers. For this study the model was rolled 90°; consequently the oil had a natural tendency to flow downward due to gravity. It should be pointed out that the oil streaks represent the direction of shear within the innermost region of the boundary layer and do not necessarily reflect the flow direction at the outer edge of the boundary layer. However, it can be assumed that the uniform, near-parallel streaks represent a flow which is essentially two-dimensional.

An examination of the flow patterns indicates that although the flow approaching the distorted section was essentially two-dimensional, the flow over the waves and beyond was not necessarily two-dimensional. For $\alpha = 0^{\circ}$, presented in figure 10, the shear forces were small and in some regions the oil dots did not move. However, as the angle of inclination increased the patterns became much more definite. The effect of the end-plate boundary layer on the two-dimensionality of the flow field becomes apparent, especially for the higher Reynolds numbers, at $\alpha = 5^{\circ}$. Irregularities in the flow ahead of and within the distorted section are clearly evident at $\alpha = 10^{\circ}$ for the higher Reynolds numbers.

Some of the irregularities in the oil patterns are believed to have been caused by vortices. The presence of vortices is indicated by the swirling of the oil at the downstream extremities of the irregularities ahead of the first wave (figs. 12(b) and (c)). The appearance of vortices on plates with and without separation regions has also been reported in reference 9 and references 15 to 20.

Boundary-layer separation.- The apparent location of the beginning of the separated flow region forward of the first wave was obtained from oil-flow studies. The effect of angle of inclination and Reynolds number on the extent of the boundary-layer separation region is presented in figure 13. As noted in figures 10, 11, and 12, the oil-flow pattern may not have been fully developed with regard to the separation line when the pictures were taken. However, the position of the oil separation lines was obtained after the photographs were taken by locating the midpoint of the oil accumulation line with a coordinate cathetometer. The bars on the symbols in figure 13 represent the irregularities in the separation line as observed in the photographs at $\alpha = 10^{\circ}$ for the higher Reynolds numbers.

For $\alpha = 0^{\circ}$, the oil did not flow enough to indicate a definite separation region. However, heat-transfer results which are discussed subsequently indicate that the flow probably did not separate ahead of the first wave for $\alpha = 0^{\circ}$.

One obvious effect of increasing the angle of inclination (decreasing the local Mach number), as shown in figure 13, was to increase the extent of the separation region (the separation point moved forward) ahead of the first wave. Also, as the Reynolds number increased, the extent of the separated region increased.

Flow-Field Survey

A pitot-pressure survey was made to obtain the local Mach number at the edge of the boundary layer for $\alpha = 0^{\circ}$, and to compare the local flow in the wavy wall section with that on the undisturbed flat plate. Results of the pitot-pressure survey from the model surface out to the undisturbed free stream are presented in figure 14 at $x = 7.6$ inches (19.3 cm) for $\alpha = 0^{\circ}$. The distance from the flat-plate surface and the local pitot pressure have been nondimensionalized by using the distance out to the leading-edge shock wave and the free-stream pitot pressure, respectively, as reference values. Surveys from the flat-plate surface and the distorted surface are compared with results of a survey made by Feldhuhn (ref. 21). A study of other surveys made by Feldhuhn at several stations indicates that the curve in figure 14, representing his most downstream position, would tend to flatten out beyond the knee of the curve and would approach the present results more closely as the survey stations approach the same $R_{\infty,x}$ value.

Since the pitot pressure varied from the wall out to the leading-edge shock because of an entropy gradient therein, the edge of the boundary layer, and consequently the local Mach number, could not be readily defined. At the edge of the schlieren boundary layer, a local Mach number of 5.4 was determined from the pitot survey and the measured wall pressure; at the boundary-layer thickness predicted by equation (2) of reference 21 the local Mach number was 8. These values are much lower than the Mach number of 14 found by using the local shock angle and the wall pressure.

For comparison purposes, the laminar boundary-layer displacement thickness δ^* found by the reference temperature method of Monoghan (ref. 22) is presented for two local conditions.

Pressure Distribution

In order to compare the effects of Reynolds number and angle of attack, the flat-plate pressure distributions have been presented in figure 15 as a function of the viscous interaction parameter λ_{∞}. Although the data are underpredicted by the viscous-induced theory of reference 23, the proper trends are indicated. An improvement in the

predictions is made at $\alpha = 0^{\circ}$ by taking the combined leading-edge bluntness and viscous effects into account (Henderson et al., ref. 24). For the highest Reynolds numbers at $\alpha = 10^{\circ}$, the slope of the data changes from positive to negative at the lowest λ_{∞}. This change may be due to a rapid increase in the boundary-layer thickness in a transitional flow region. The inviscid wedge pressures (ref. 14) are also indicated in figure 15 for $\alpha = 5^{\circ}$ and 10°.

The pressure distributions from the flat plate and distorted sections are compared in figure 16. These data are presented for three angles of inclination at constant free-stream Mach numbers and unit Reynolds numbers. Although pressure data were obtained at several spanwise locations (see fig. 4 and table II) there were no discernible span effects noted in the pressure measurements; therefore, the spanwise locations of the orifices are not indicated in figure 16.

In the region of surface distortions, the values of the pressure ratio oscillate from maximum to minimum as a result of the surface waves and are modified by boundary-layer separation and reattachment. The pressure ratio increased ahead of the first wave in all cases and, although the flow was separated for $\alpha = 5^{\circ}$ and 10° (the separation point as indicated by the oil-flow studies is noted in fig. 16), no plateau pressures were clearly indicated.

Immediately downstream of the last protuberance the flow expanded to a pressure level much lower than that for the preceding waves. However, the pressures tend to rise toward the undisturbed flat-plate values farther downstream. These low pressure levels immediately downstream of the distorted section were also obtained by Rhudy and Magnan (ref. 6) and by Bertram and his coworkers (ref. 8).

The magnitude of the pressure oscillations does not decrease with distance for the investigations at a 10° angle of incidence as it does for lower angles. A rise in peak pressure ratio toward the end of the distorted region is noted at the higher Reynolds numbers, and for the highest Reynolds number (see fig. 16(c)), the last two peak pressure values are much larger with respect to the average value. This increase in peak pressure is believed to be due to transition of the boundary layer; transition is also substantiated by the heat-transfer results which are presented subsequently.

In order to compare the relative locations and magnitudes of the maximum and minimum pressures, these values have been presented in figure 17. The maximum pressures occurred just ahead of the "peak" of the protuberances and moved slightly rearward for the 5° and 10° angles of inclination. Similarly, the minimum pressures occurred just ahead of the bottom of the depressions and moved slightly rearward at the higher angles of inclination. The changes in Reynolds number had very little effect on the maximum and minimum levels except that the maximum pressures in the region downstream of the second wave at $\alpha = 10^{\circ}$ increased as a result of transition within the boundary layer.

Reference 6 shows the same behavior for flow with transition in the boundary layer in the region where there are surface distortions. It is apparent that the type of boundary layer (laminar or transitional) was the factor which had the greatest effect on the pressure rise for the range of variables covered in this investigation.

Comparisons of the maximum pressures measured on the first wave with the Savage-Nagel theory (ref. 7) are shown in figure 18. The pressures are presented as a function of angle of inclination, since the maximum pressure depends on both the local Mach number and the boundary-layer displacement thickness. It should be pointed out that the theory was developed for attached laminar flow; this condition applied only for $\alpha = 0^{\circ}$, where the theory was in agreement with the data (within the accuracy of the data). Although the shallow-wave theory predicted an increase in the maximum pressures with increasing angle of inclination, the actual increases of the experimental values were less. Also, the theoretical spread in the pressure level was not observed in the data.

Heat-Transfer Distribution

As shown in figure 19, the laminar flat-plate heat-transfer distributions can be adequately predicted by the theory of Bertram and Feller (ref. 25), which accounts for pressure level and gradient. The theory for zero pressure gradient is also shown for comparison. The sharp rise in heating with distance from the leading edge for $\alpha = 10^{\circ}$ is indicative of a change from laminar to transitional flow within the boundary layer.

The nondimensional heat-transfer distributions over the flat plate and distorted sections are compared in figure 20. The heat-transfer data were obtained at several spanwise locations (see fig. 4 and table I); these locations are indicated in figure 20.

In the region of surface distortions the values of Stanton number oscillate from maximum to minimum as a result of the wavy surface and are altered by boundary-layer separation and reattachment. The general shape of the heat-transfer distributions in the separated region ahead of the first wave agrees with that obtained by Jaeck (ref. 7) and, in general, with that of Needham (ref. 26). In the present investigation, the heat transfer decreased in the separated regions ahead of the first wave for $\alpha = 5^{\circ}$ and 10°, and the minimum value occurred downstream of the separation point and ahead of the wave. This same situation was noted by Needham for separation due to a compression wedge. Rhudy and Magnan found that at a Mach number of 10 and the lowest Reynolds number of their tests (0.042×10^6 per inch or 0.016×10^6 per cm), the minimum value of heat transfer occurred on the first wave of a sine-wave distortion section. (See ref. 6.)

It should be noted that the apparent scatter in Stanton number ahead of the first wave for the highest Reynolds number at $\alpha = 10^{\circ}$ was probably caused by vortices observed in this region in the oil-flow studies (see fig. 12).

The Stanton number decreased to well below the flat-plate level immediately downstream of the last protuberance, which was also the point at which a sharp decrease in pressure was noted (see fig. 16), except for $\alpha = 0^{\circ}$. For $\alpha = 0^{\circ}$ the minimum heating occurred just aft of the crest on the wave itself; however, the heat-transfer levels generally tended to return to the undisturbed flat-plate values a short distance downstream of the distorted section.

The relative positions and magnitudes of the maximum and minimum heat-transfer levels are shown in figure 21. All the maximum Stanton numbers occurred just ahead of the peak of the protuberances, while the minimum values were measured just before the bottom of the depressions; these locations did not change over the range of the test conditions. The heating in the distorted region varied by as much as a factor of 50 when both laminar and transitional flow were present.

Maximum wave heating as predicted by the laminar shallow-wave theory (ref. 7) is shown in figure 22, where the maximum laminar heating in the distorted section is plotted as a function of the ratio of the protuberance height to laminar-boundary-layer displacement thickness (ref. 22). The shallow-wave theory predictions are presented for local Mach numbers obtained from oblique-shock tables (ref. 14) by using ratios of measured local pressure to free-stream static pressure. However, for $M_{\infty} = 8$ and $\alpha = 0^{\circ}$, the experimental Mach number obtained from the flow-field survey presented in figure 14 was used.

The shallow-wave theory should apply only to a shallow wave in attached laminar flow; that is, the first wave for $\alpha = 0^{\circ}$. In figure 22 there is good agreement between the theory and the results for $\alpha = 0^{\circ}$ at the lowest unit Reynolds number, but at the higher first-wave Reynolds numbers the maximum heating values are underpredicted. Data for the successive waves at $\alpha = 0^{\circ}$ for the lowest unit Reynolds number are in fair agreement with the theory. However, the rest of the data are too widely scattered to suggest any trend.

Maximum-heating correlation parameters incorporating the local Mach number and displacement thickness have been suggested by Bertram and his coworkers in reference 8. These parameters have been used in figure 23 to correlate the first-wave maximum heating for the present tests and the results in air at a Mach number of 10.1 from reference 7. Although there is a large spread in the data, the maximum heating on the first wave generally correlates for the different angles of inclination, and the air and helium results are in fair agreement. The lack of complete correlation of the results (independent of α) may be due to the fact that the actual local values are not known. The large discrepancies that can be introduced due to an incomplete knowledge of the local flow conditions are illustrated by the difference in the correlation parameters based on the calculated and the experimental local Mach number for $\alpha = 0^{\circ}$. Considerable scatter

was also evident in results of similar tests reported in reference 8, but the scatter did not appear to be a function of M_∞, M_l, R_∞, or $H/\delta_l{}^*$. A general fit to the laminar first-peak air data was represented by the equation

$$\frac{h_{max}}{h_l} = 1 + \frac{1}{36}\left(\frac{M_l}{\delta^*/H}\right)^{1.9} \tag{4}$$

which is shown in figure 23 for comparison.

CONCLUDING REMARKS

An experimental investigation was conducted to determine the effects of a two-dimensional repetitive sine-wave distortion on the pressure and heat-transfer distributions. Tests were made on a sharp flat plate with a distorted section in a relatively thick boundary layer which changed from laminar to transitional for certain test conditions. The tests were conducted in helium at free-stream Mach numbers of about 20, over a range of length Reynolds numbers varying from 2.72×10^6 to 8.80×10^6 with the flat-plate surface at angles of inclination of 0°, 5°, and 10°.

The results of the present tests were similar to results obtained in air at lower free-stream Mach numbers and Reynolds numbers with relatively thinner boundary layers. The pressure and heat-transfer distributions were greatly altered in the distorted section (oscillating from maximum to minimum values) with the heating distribution being affected the most. The magnitude of these pressure and heat-transfer oscillations also depended on whether the flow was laminar or transitional. However, the values generally approached the undisturbed flat-plate results a short distance downstream of the distorted region.

The Savage-Nagel attached laminar-flow theory for shallow waves adequately predicted the first-wave maximum pressures for attached laminar flow. However, the theory was not routinely successful in predicting the first-wave maximum pressures in separated flow and the first-wave maximum heat-transfer results for attached and separated laminar flow. For different angles of attack, the first-wave maximum laminar heating was correlated with results obtained in air in a previous Mach 10 investigation.

When the boundary layer was transitional, vortices were indicated in the separated flow regions by surface oil-flow studies. These were not observed in the laminar case.

Langley Research Center,
National Aeronautics and Space Administration,
Langley Station, Hampton, Va., August 12, 1968,
126-13-03-25-23.

REFERENCES

1. Chapman, Dean R.; Kuehn, Donald M.; and Larson, Howard K.: Investigation of Separated Flows in Supersonic and Subsonic Streams With Emphasis on the Effect of Transition. NACA Rep. 1356, 1958. (Supersedes NACA TN 3869.)

2. Sterrett, James R.; and Emery, James C.: Extension of Boundary-Layer-Separation Criteria to a Mach Number of 6.5 by Utilizing Flat Plates With Forward-Facing Steps. NASA TN D-618, 1960.

3. Putnam, Lawrence E.: Investigation of Effects of Ramp Span and Deflection Angle on Laminar Boundary-Layer Separation at Mach 10.03. NASA TN D-2833, 1965.

4. Shore, Charles P.; Dixon, Sidney C.; and Griffith, George E.: Experimental Pressures and Turbulent Heat-Transfer Coefficients Associated With Sinusoidal Protuberances on a Flat Plate at a Mach Number of 3. NASA TN D-1626, 1963.

5. Bertram, Mitchel H.; and Wiggs, M. Margarette: Effect of Surface Distortions on the Heat Transfer to a Wing at Hypersonic Speeds. AIAA J., vol. 1, no. 6, June 1963, pp. 1313-1319.

6. Rhudy, J. P.; and Magnan, J. D.: Investigation of Heat Transfer and Pressure Distributions in Regions of Surface Distortion on a Flat Plate. AEDC-TDR-62-238, U.S. Air Force, Jan. 1963.

7. Jaeck, C. L.: Analysis of Pressure and Heat Transfer Tests on Surface Roughness Elements With Laminar and Turbulent Boundary Layers. NASA CR-537, 1966.

8. Bertram, M. H.; Weinstein, L. M.; Cary, A. M., Jr.; and Arrington, J. P.: Heat Transfer to Wavy Wall in Hypersonic Flow. AIAA J., vol. 5, no. 10, Oct. 1967, pp. 1760-1767.

9. Cary, A. M., Jr.; and Morrisette, E. L.: Effect of Two-Dimensional Multiple Sine-Wave Protrusions on the Pressure and Heat-Transfer Distributions for a Flat Plate at Mach 6. NASA TN D-4437, 1968.

10. Mechtly, E. A.: The International System of Units – Physical Constants and Conversion Factors. NASA SP-7012, 1964.

11. Arrington, James P.; Joiner, Roy C., Jr.; and Henderson, Arthur, Jr.: Longitudinal Characteristics of Several Configurations at Hypersonic Mach Numbers in Conical and Contoured Nozzles. NASA TN D-2489, 1964.

12. O'Sullivan, William J., Jr.: Some Thermal and Mechanical Properties of Inconel at High Temperatures for Use in Aerodynamic Heating Research. Proc. A.S.T.M., vol. 55, 1965, pp. 757-763.

13. Nicoll, K. M.: Investigation of the Laminar Boundary Layer on a Flat Plate in Helium Using the Crocco Method. ARL 62-345, U.S. Air Force, May 1962.

14. Henderson, Arthur, Jr.; and Braswell, Dorothy O.: Charts for Conical and Two-Dimensional Oblique-Shock Flow Parameters in Helium at Mach Numbers From About 1 to 100. NASA TN D-819, 1961.

15. Miller, D. S.; Hijman, R.; and Childs, M. E.: Mach 8 to 22 Studies of Flow Separation Due to Deflected Control Surfaces. AIAA J., vol. 2, no. 2, Feb. 1964, pp. 312-321.

16. Hopkins, Edward J.; Keating, Stephen J., Jr.; and Bandettini, Angelo: Photographic Evidence of Streamwise Arrays of Vortices in Boundary-Layer Flow. NASA TN D-328, 1960.

17. Ginoux, Jean J.: Experimental Evidence of Three-Dimensional Perturbations in the Reattachment of a Two-Dimensional Laminar Boundary-Layer at Mach = 2.05. Tech. Note 1 (Contract AF 61(514)-993), Training Center Exp. Aerodyn. (Belgium), Nov. 1958.

18. Ginoux, Jean J.: Leading-Edge Effect on Separated Supersonic Flows. Proceedings of the Third Congress of the International Council of the Aeronautical Sciences, Spartan Books, Inc., 1964, pp. 421-431.

19. Ginoux, J. J.: Laminar Separation in Supersonic Flow. AFOSR 65-0352, U.S. Air Force, Oct. 1964. (Available from DDC as AD 612 407.)

20. Ginoux, Jean J.: Investigation of Flow Separation Over Ramps at $M_\infty = 3$. AEDC TR-65-273, U.S. Air Force, Dec. 1965. (Available from DDC as AD 475242.)

21. Feldhuhn, Robert H.: An Experimental Investigation of the Effects of Leading Edge Reynolds Number and Angle of Attack on the Flow of Helium Over a Flat Plate at M = 16.35. Gas Dyn. Lab. Intern. Mem. 8, Princeton Univ., July 1965.

22. Monaghan, R. J.: An Approximate Solution of the Compressible Laminar Boundary Layer on a Flat Plate. R. & M. No. 2760, Brit. A.R.C., 1953.

23. Bertram, Mitchel H.: Hypersonic Laminar Viscous Interaction Effects on the Aerodynamics of Two-Dimensional Wedge and Triangular Planform Wings. NASA TN D-3523, 1966.

24. Henderson, Arthur, Jr.; Watson, Ralph D.; and Wagner, Richard D., Jr.: Fluid Dynamic Studies to M = 41 in Helium. AIAA J., vol. 4, no. 12, Dec. 1966, pp. 2117-2124.

25. Bertram, Mitchel H.; and Feller, William V.: A Simple Method for Determining Heat Transfer, Skin Friction, and Boundary-Layer Thickness for Hypersonic Laminar Boundary-Layer Flows in a Pressure Gradient. NASA MEMO 5-24-59L, 1959.

26. Needham, David A.: A Heat-Transfer Criterion for the Detection of Incipient Separation in Hypersonic Flow. AIAA J. (Tech. Notes), vol. 3, no. 4, Apr. 1965, pp. 781-783.

TABLE I.- LOCATION OF THERMOCOUPLES

(a) Flat surface

x		Row	x		Row
in.	cm		in.	cm	
2.171	5.51	E	8.171	20.75	E
3.171	8.05	E	8.671	22.02	F
3.671	9.32	G	9.171	23.29	G
4.171	10.59	E	10.171	25.83	E
4.671	11.86	G	11.171	28.37	G
5.171	13.13	E	12.171	30.91	E
6.171	15.67	E	13.171	33.45	G
6.671	16.94	G	14.171	35.99	A, B, E
7.171	18.21	E	15.171	38.53	G
7.671	19.48	G			

(b) Distorted surface

x		Row	x		Row
in.	cm		in.	cm	
2.050	5.21	D	8.200	20.83	H
2.550	6.48	F	8.375	21.27	D
3.050	7.75	D	8.500	21.59	F
3.300	8.38	F, J, L	8.725	22.16	H
3.550	9.02	H	8.900	22.61	D
3.800	9.65	D	9.125	23.18	F, J, L
4.300	10.92	F	9.525	24.19	H
4.550	11.56	H	9.700	24.64	D
4.800	12.19	D	9.875	25.08	F
5.025	12.76	F	10.225	25.97	H
5.100	12.95	H	10.400	26.42	D
5.200	13.21	D	10.625	26.99	F
5.375	13.65	F	11.145	28.31	D
5.500	13.97	H	11.235	28.54	F
5.725	14.54	D	11.375	28.89	H
5.900	14.99	F	11.515	29.25	D
6.125	15.56	H	11.800	29.97	F
6.525	16.57	D	12.050	30.61	H
6.700	17.02	F	12.300	31.24	D
6.875	17.46	H	12.550	31.88	F
7.225	18.35	D	13.550	34.42	D
7.400	18.80	F	14.050	35.69	F
7.625	19.37	H	14.550	36.96	H
8.025	20.38	D	15.050	38.23	D
8.100	20.57	F	15.550	39.50	F, J, K, L

TABLE II.- LOCATION OF PRESSURE ORIFICES

(a) Flat surface

x		Row	x		Row
in.	cm		in.	cm	
1.447	3.68	G	9.185	23.33	C
2.198	5.58	E	11.193	28.43	I
4.172	10.60	I	14.180	36.02	E
5.172	13.14	G	15.189	38.58	D
7.179	18.23	E			

(b) Distorted surface

x		Row	x		Row
in.	cm		in.	cm	
2.827	7.18	I	8.825	22.42	G
3.327	8.45	F	8.993	22.84	E
3.573	9.08	D	9.228	23.44	I
3.822	9.71	H	9.614	24.42	F
4.421	11.23	E	9.794	24.88	D
4.668	11.86	C	9.974	25.33	H
4.934	12.53	G	10.336	26.25	E
5.124	13.01	F	10.726	27.24	G
5.298	13.46	D	11.120	28.24	F
5.481	13.92	H	11.292	28.68	D
5.829	14.81	G	11.469	29.13	H
5.992	15.22	E	11.718	29.76	G
6.229	15.82	H	11.975	30.42	E
6.621	16.82	F	12.226	31.05	F
6.802	17.28	D	12.725	32.32	H
6.970	17.70	H	13.224	33.59	I
7.321	18.60	E	13.726	34.86	F
7.483	19.01	C	14.223	36.13	C
7.730	19.63	G	14.738	37.43	I
8.120	20.62	F	15.228	38.68	F
8.290	21.06	D	15.630	39.70	C
8.473	21.52	H			

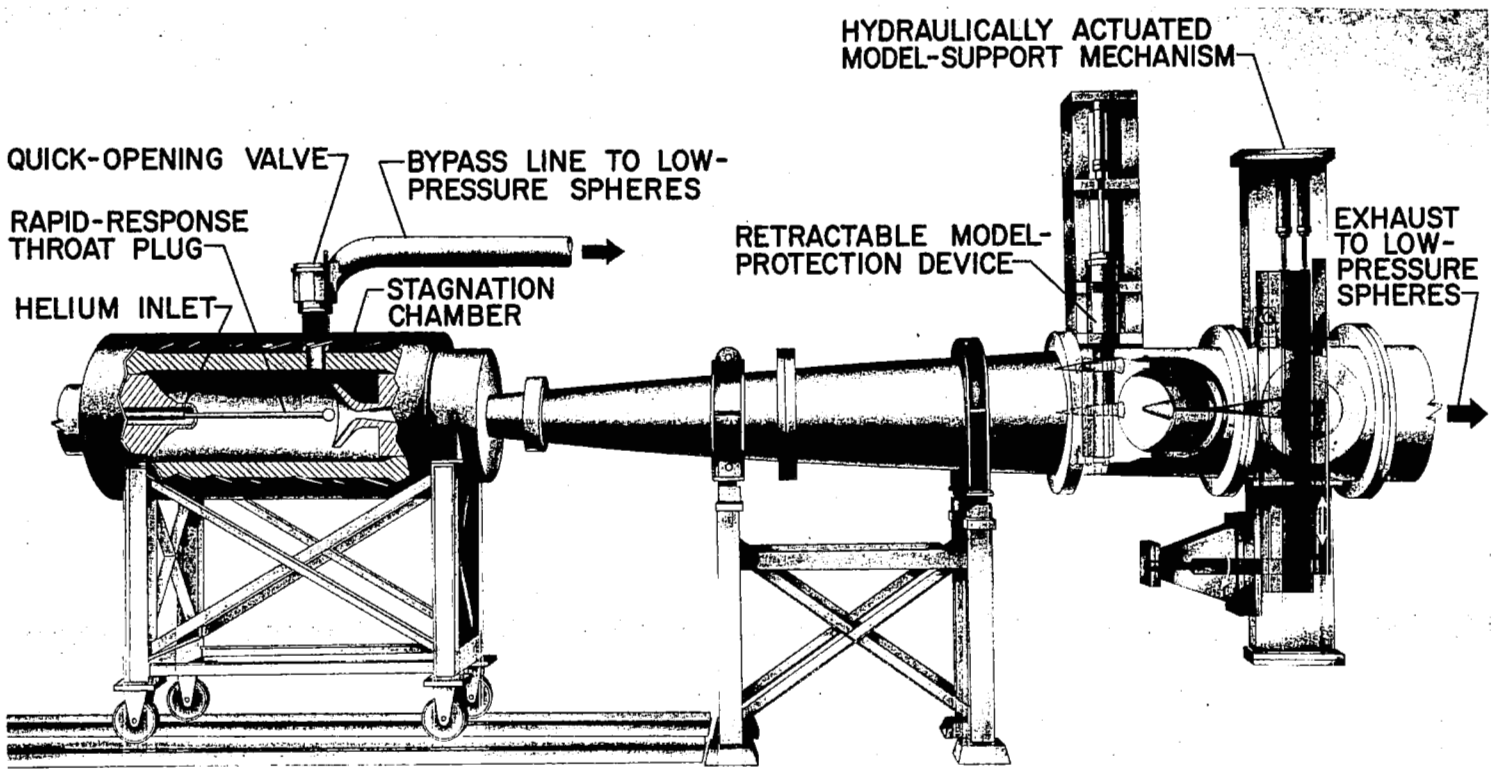

Figure 1.- Langley 22-inch helium tunnel.

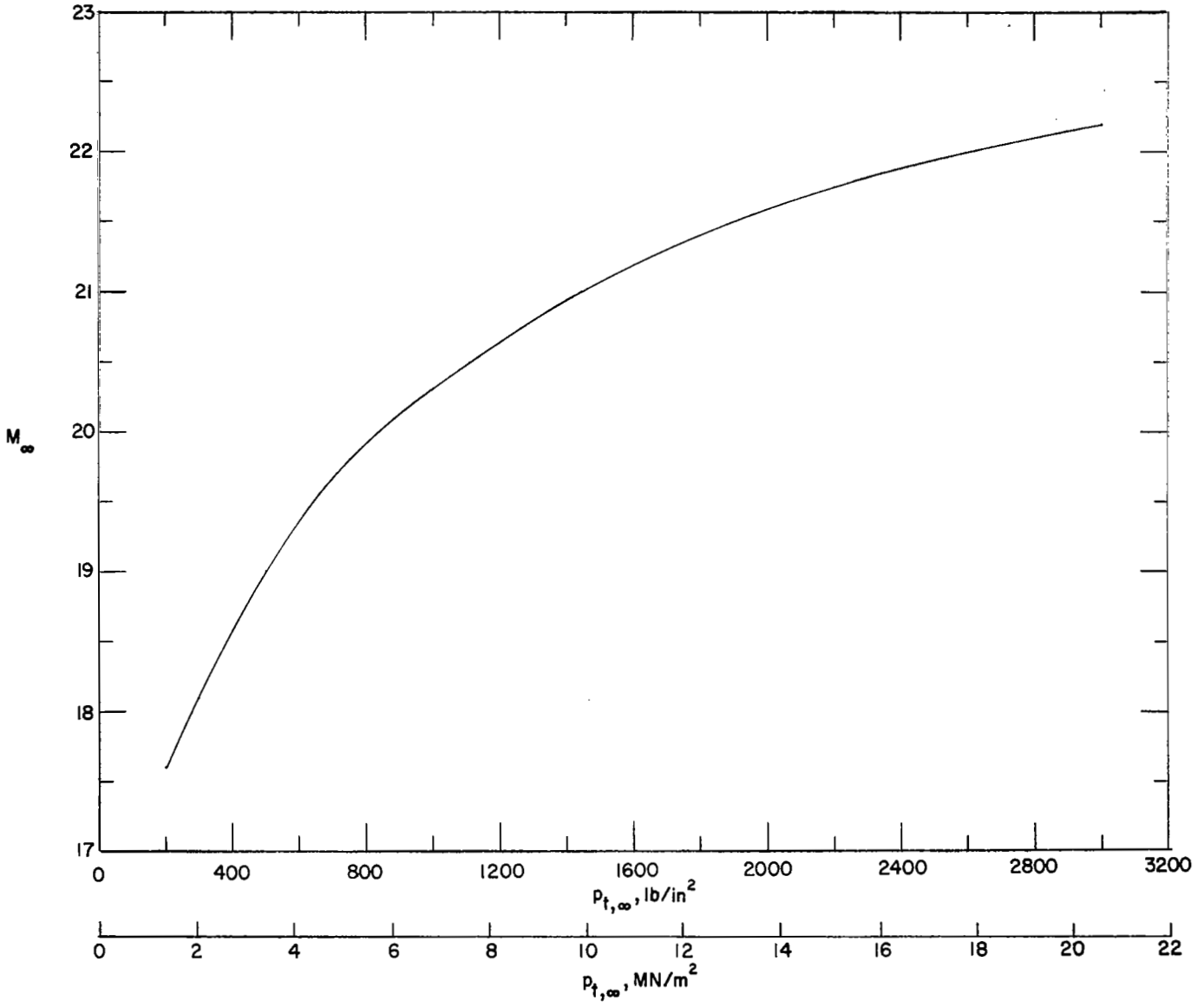

Figure 2.- Calibration summary of the average Mach number with changing stagnation pressure in the contoured nozzle with a throat diameter of 0.622 inch (1.58 cm).

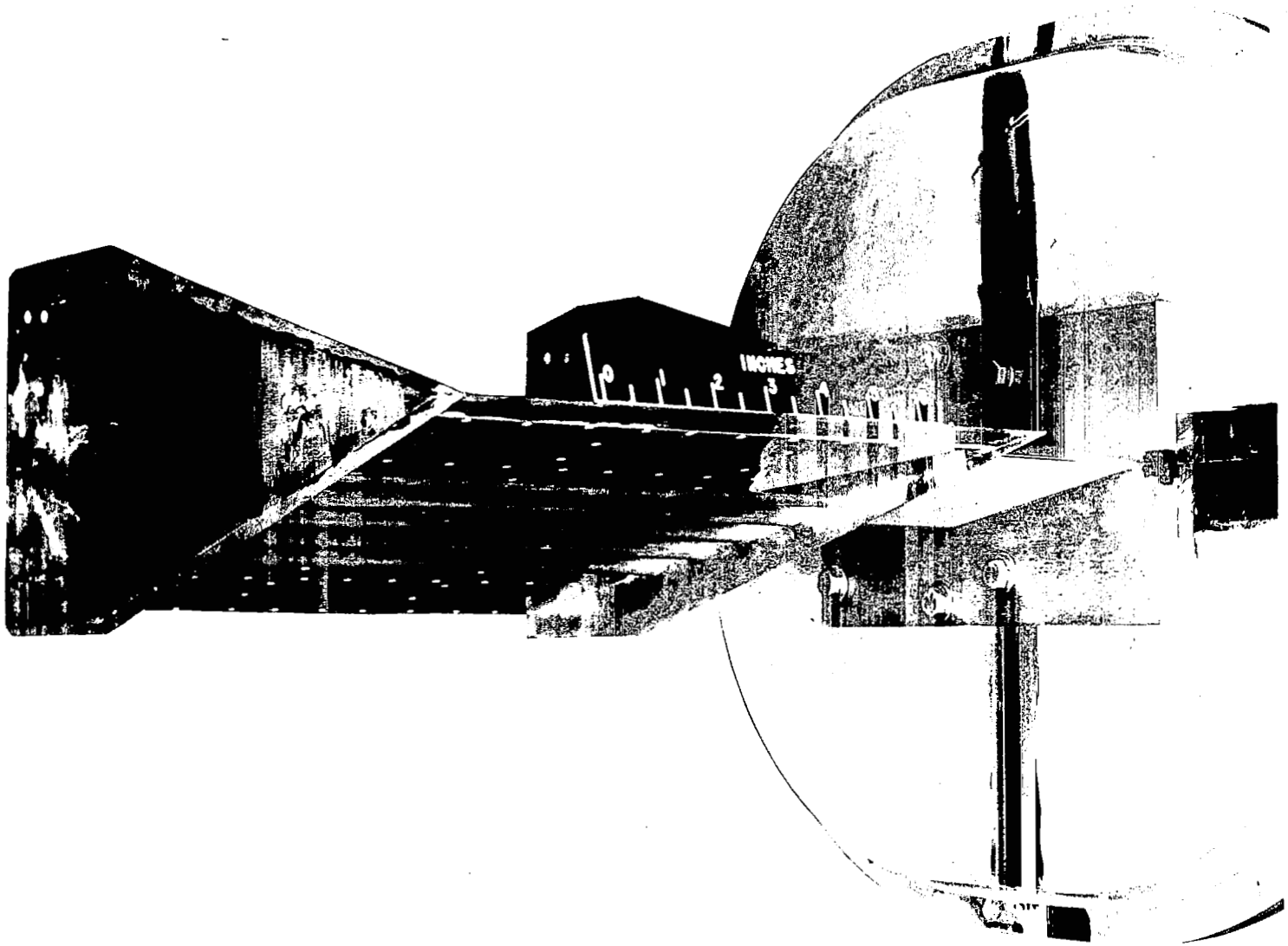

Figure 3.- Photograph of the assembled heat-transfer model.

L-68-8506

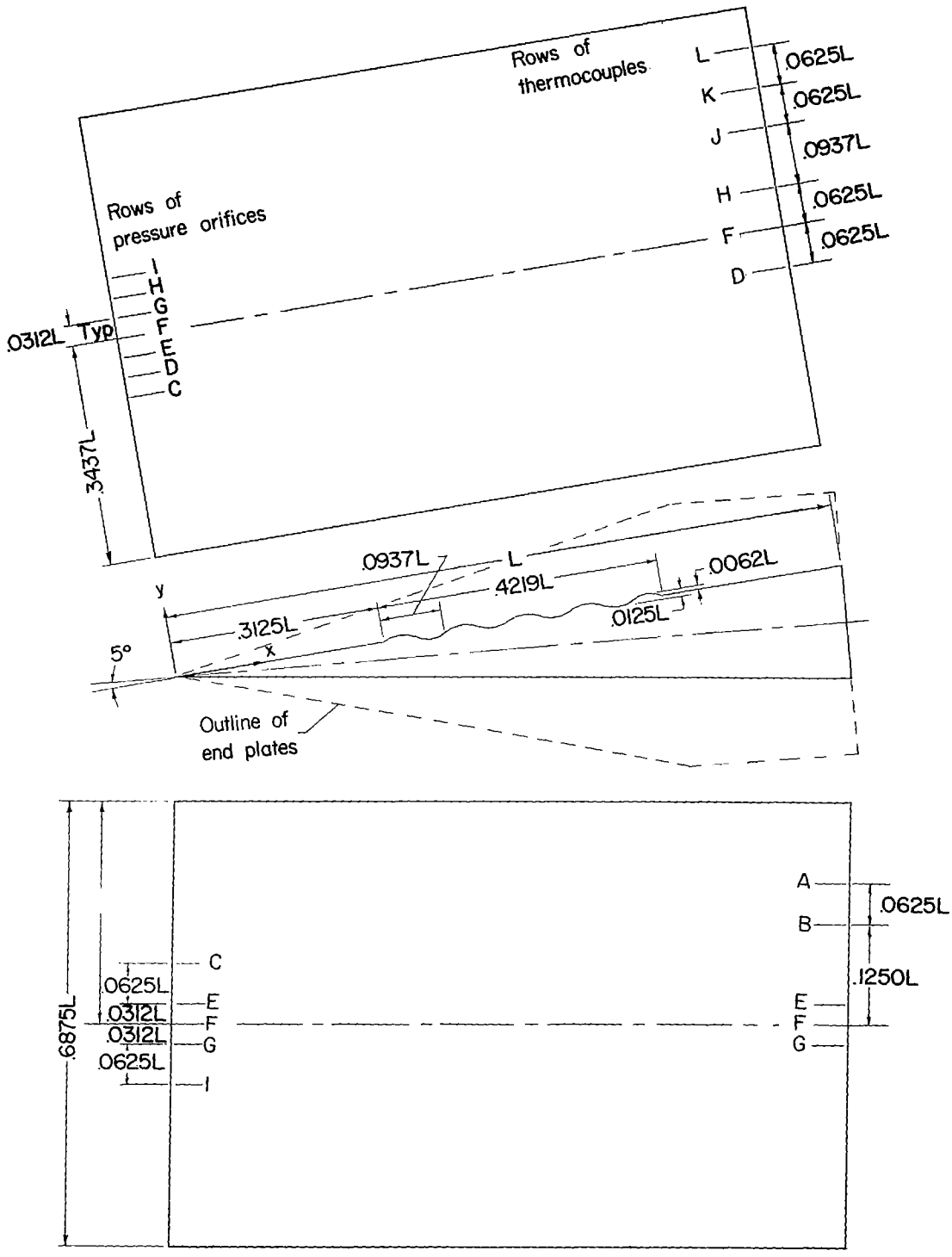

Figure 4.- Details of model and location of rows along which the pressure orifices and thermocouples were placed. All dimensions are in terms of length L (16 in. or 40.64 cm).

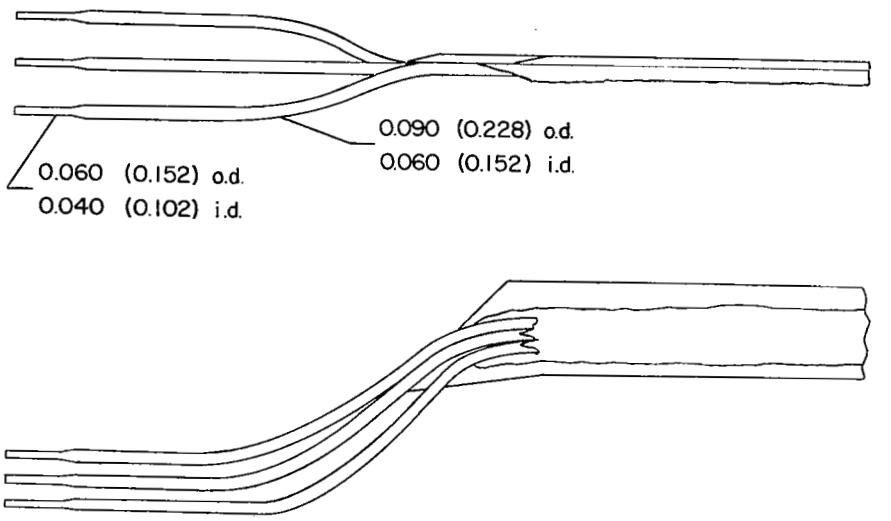

Figure 5.- Boundary-layer pitot-pressure survey rake. All dimensions are in inches (cm).

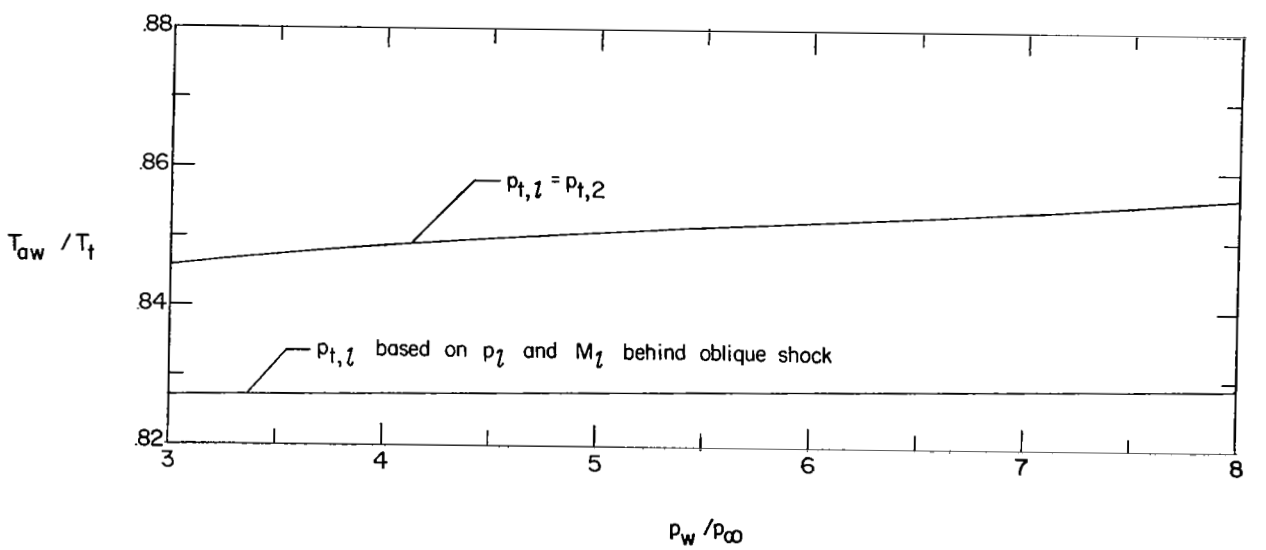

Figure 6.- Effect of local total pressure on the calculated adiabatic-wall temperature (eq. (3)) at $\alpha = 0^\circ$.

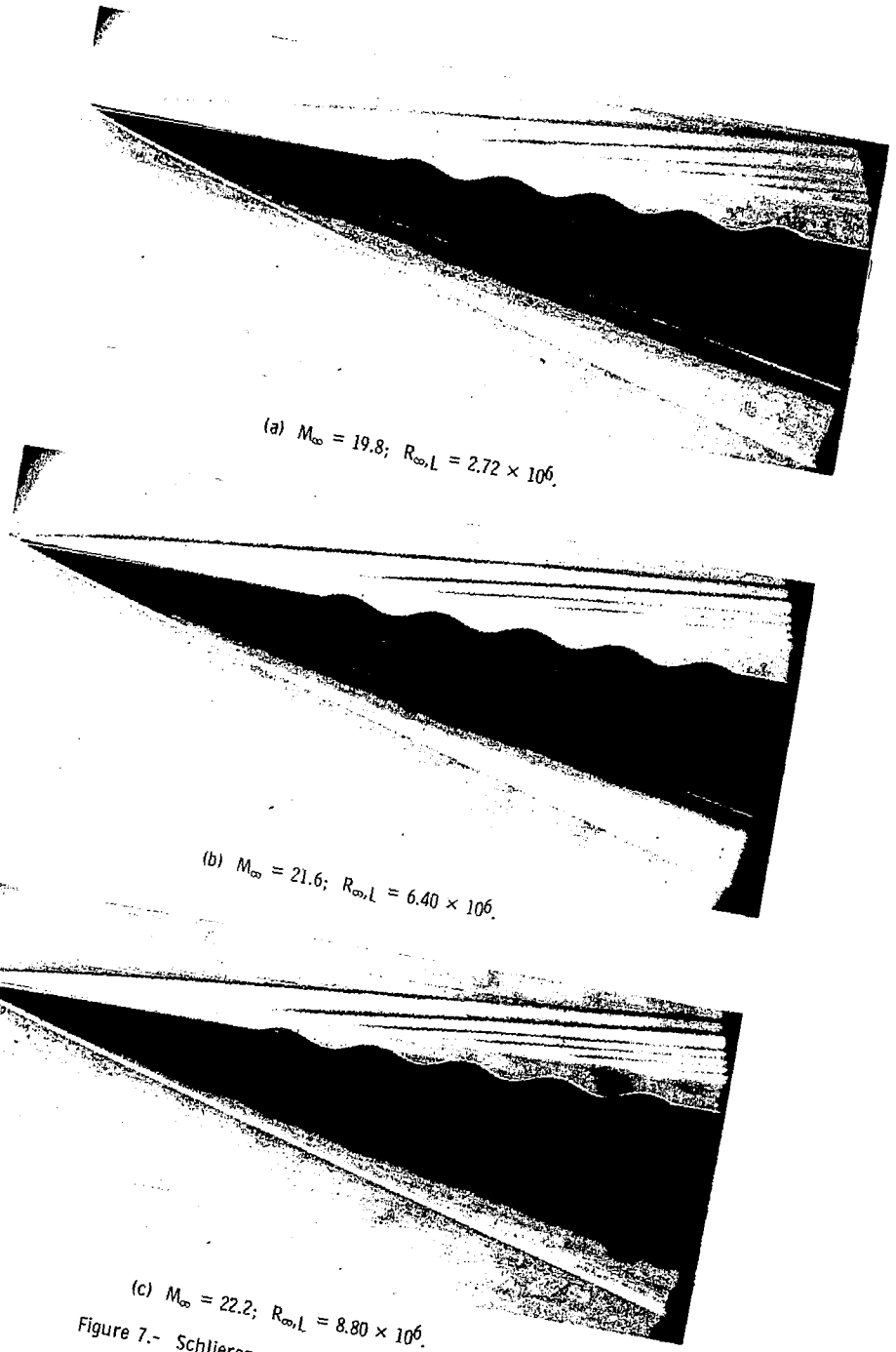

(a) $M_\infty = 19.8$; $R_{\infty,L} = 2.72 \times 10^6$.

(b) $M_\infty = 21.6$; $R_{\infty,L} = 6.40 \times 10^6$.

(c) $M_\infty = 22.2$; $R_{\infty,L} = 8.80 \times 10^6$.

Figure 7.- Schlieren photographs for $\alpha = 0^o$.

L-68-8507

(a) $M_\infty = 19.8$; $R_{\infty,L} = 2.72 \times 10^6$.

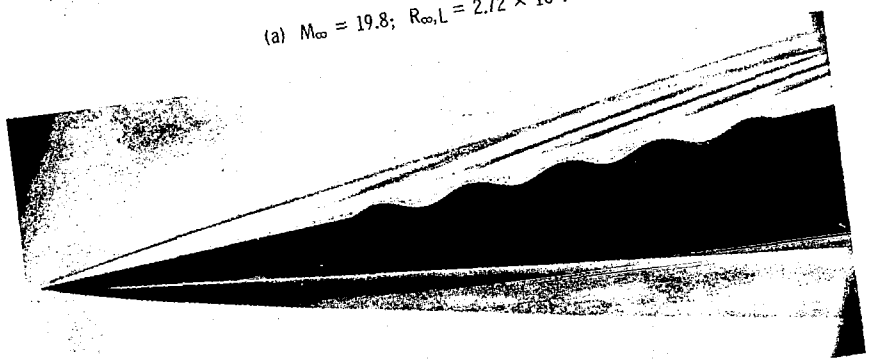

(b) $M_\infty = 21.6$; $R_{\infty,L} = 6.40 \times 10^6$.

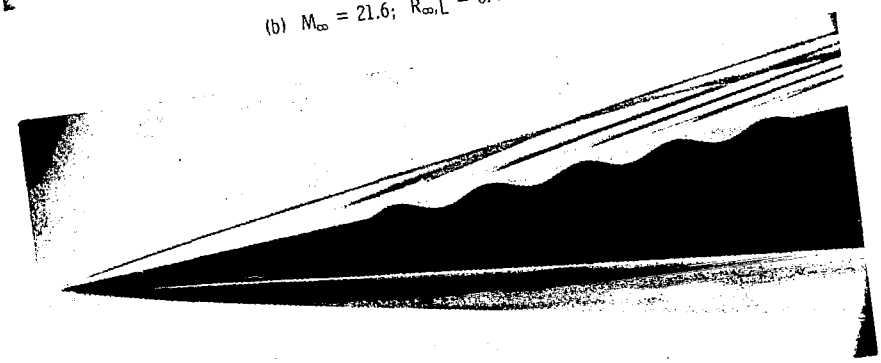

(c) $M_\infty = 22.2$; $R_{\infty,L} = 8.80 \times 10^6$.

L-68-8508

Figure 8.- Schlieren photographs for $\alpha = 5^0$.

(a) $M_\infty = 19.8$; $R_{\infty,L} = 2.72 \times 10^6$.

(b) $M_\infty = 21.6$; $R_{\infty,L} = 6.40 \times 10^6$.

(c) $M_\infty = 22.2$; $R_{\infty,L} = 8.80 \times 10^6$.

Figure 9.- Schlieren photographs for $\alpha = 10^0$.

L-68-8509

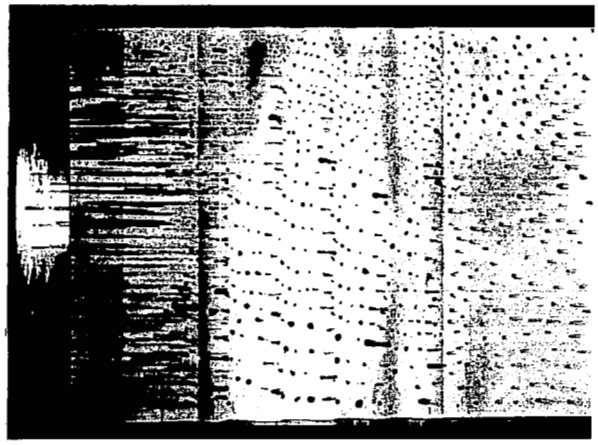

(a) $M_\infty = 19.8$; $R_{\infty,L} = 2.72 \times 10^6$.

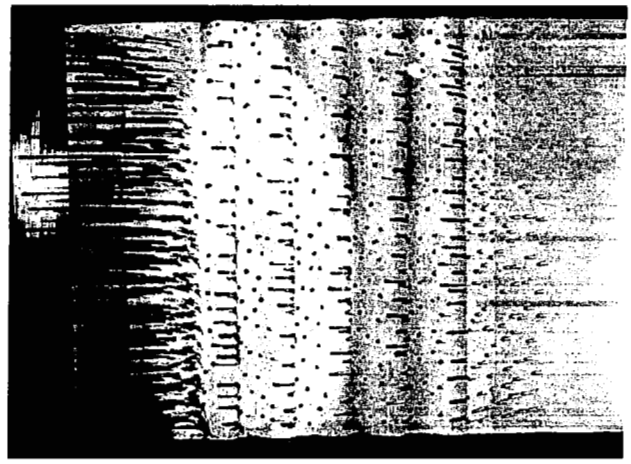

(b) $M_\infty = 21.6$; $R_{\infty,L} = 6.40 \times 10^6$.
(Oil flow not fully established.)

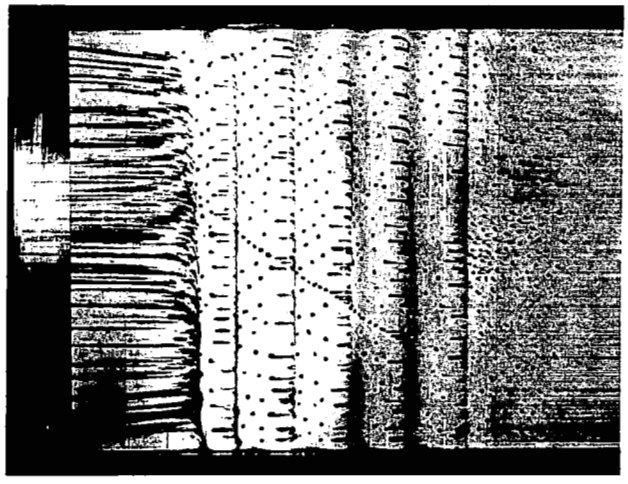

(c) $M_\infty = 22.2$; $R_{\infty,L} = 8.80 \times 10^6$.

Figure 10.- Oil-flow studies for $\alpha = 0^0$. Model is mounted in the vertical plane. L-68-8510

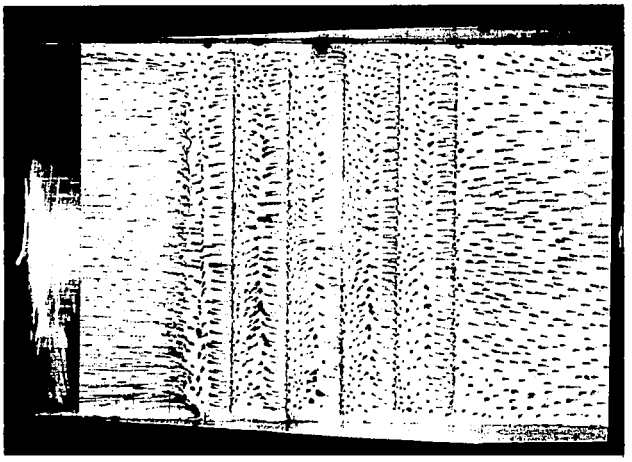

(a) $M_\infty = 19.8$; $R_{\infty,L} = 2.72 \times 10^6$.
(Oil flow not fully established.)

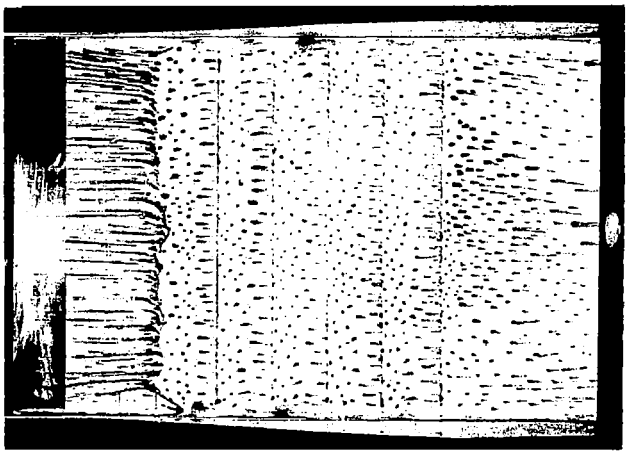

(b) $M_\infty = 21.6$; $R_{\infty,L} = 6.40 \times 10^6$.

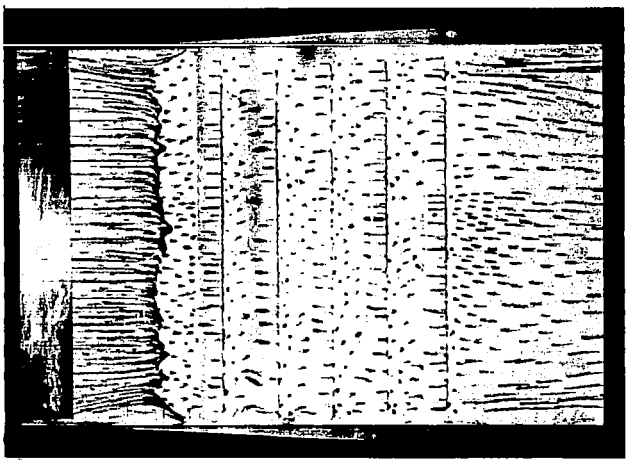

(c) $M_\infty = 22.2$; $R_{\infty,L} = 8.80 \times 10^6$.

Figure 11.- Oil-flow studies for $\alpha = 5^0$. Model is mounted in the vertical plane. L-68-8511

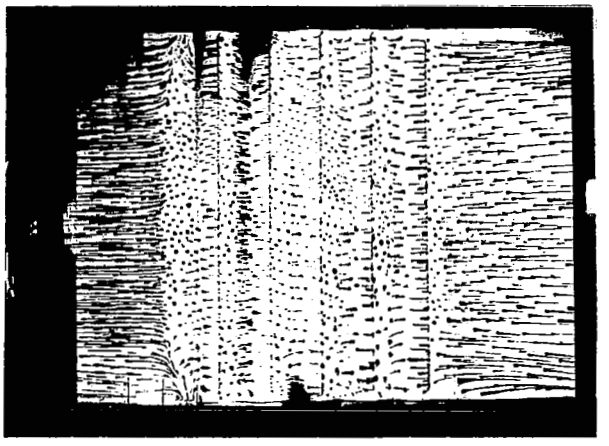

(a) $M_\infty = 19.8$; $R_{\infty,L} = 2.72 \times 10^6$. (Oil flow not fully established.)

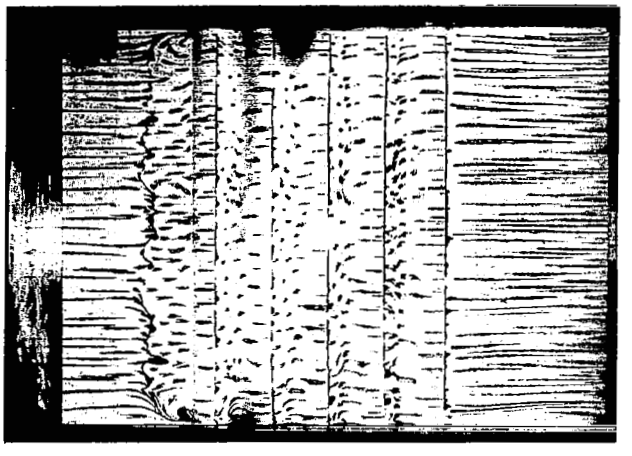

(b) $M_\infty = 21.6$; $R_{\infty,L} = 6.40 \times 10^6$.

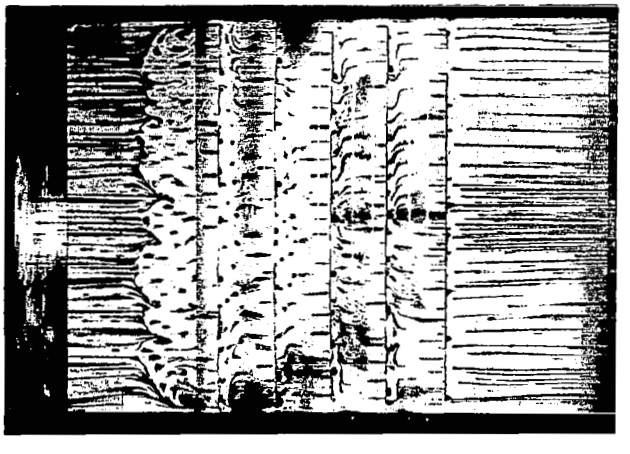

(c) $M_\infty = 22.2$; $R_{\infty,L} = 8.80 \times 10^6$.

Figure 12.- Oil-flow studies for $\alpha = 10^0$. Model is mounted in the vertical plane. L-68-8512

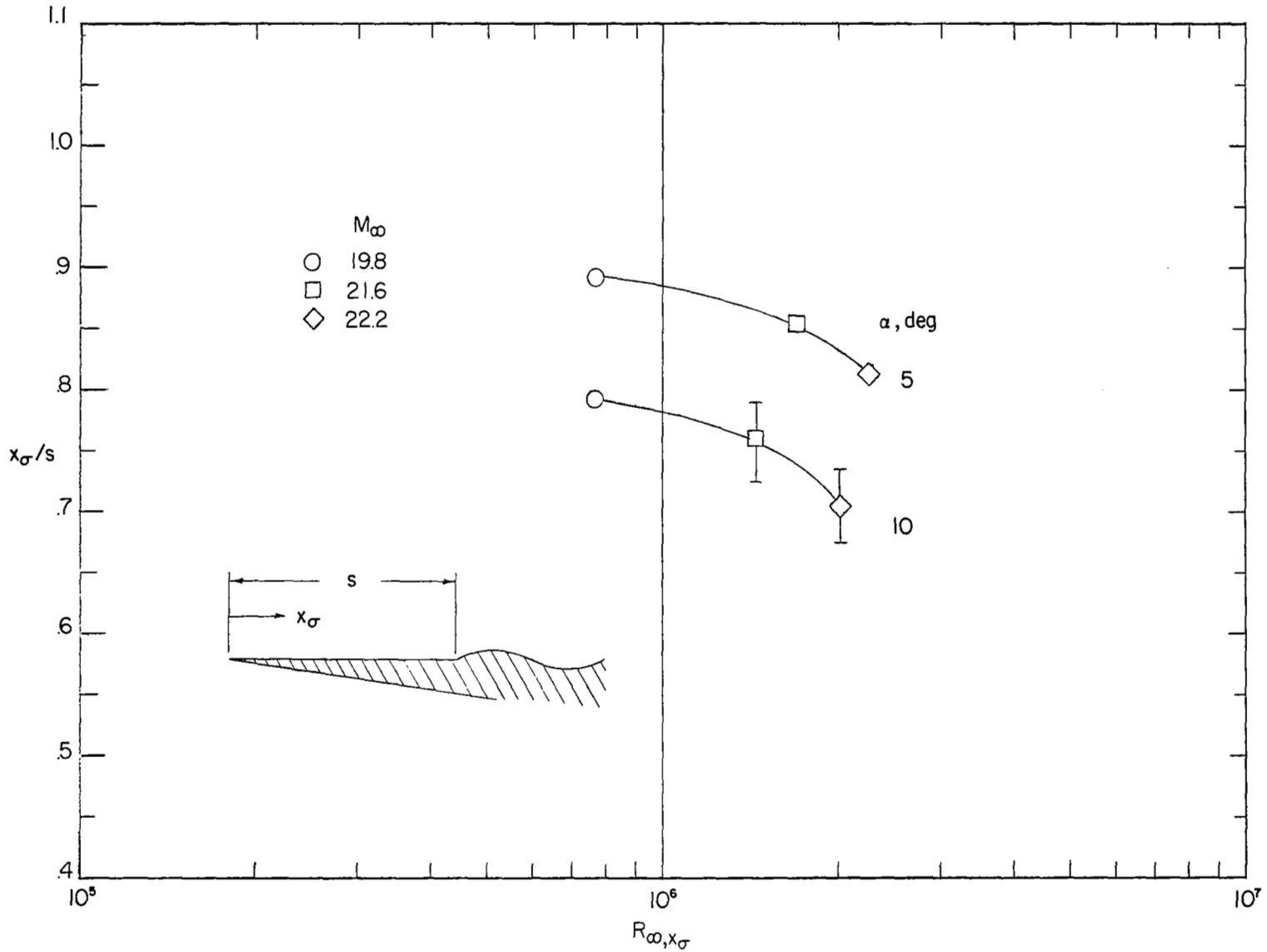

Figure 13.- Separation ahead of first wave as indicated by oil-flow studies. Bars indicate the irregularity of the oil-flow separation line.

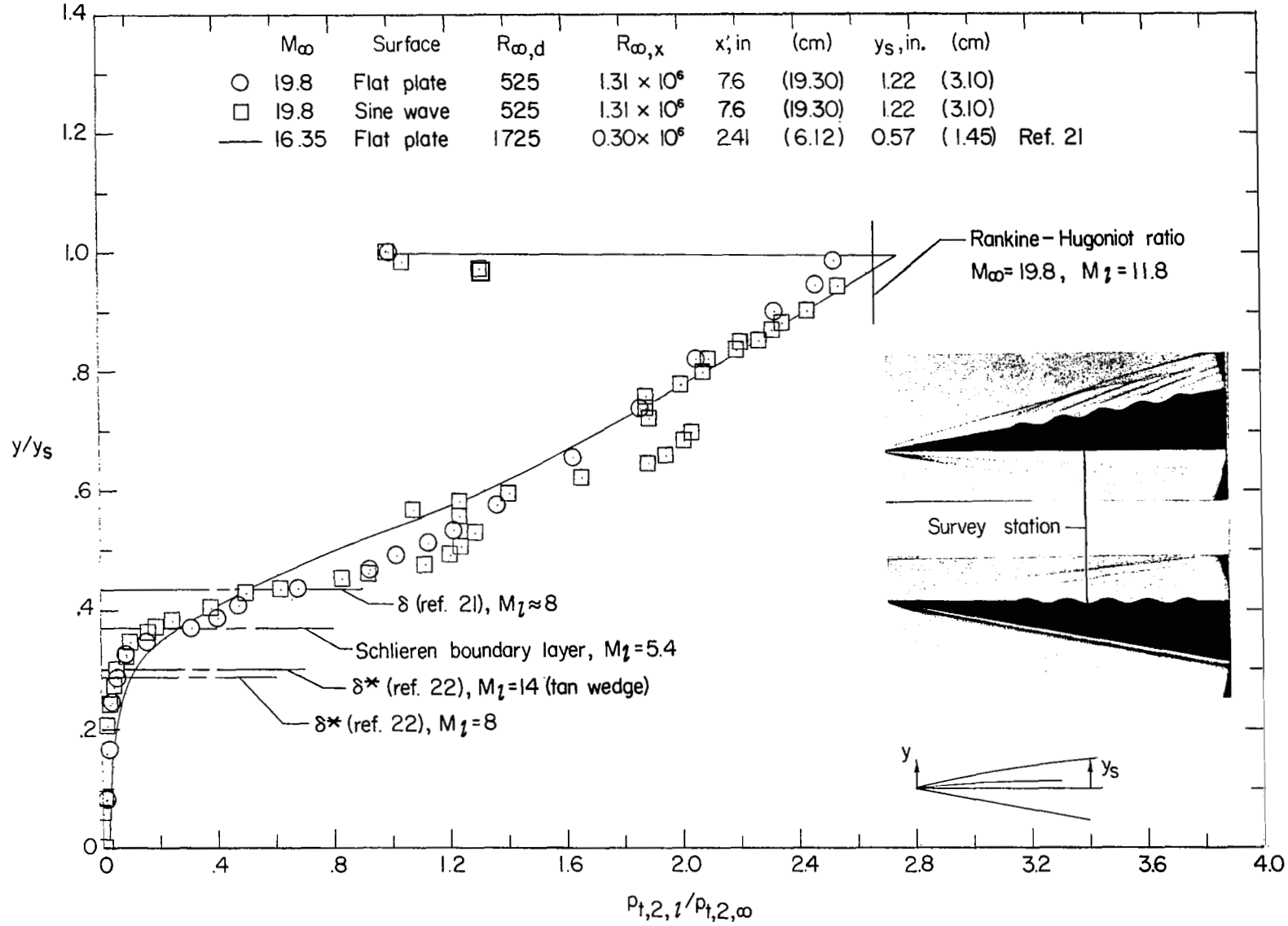

Figure 14.- Pitot-pressure profile for $\alpha = 0^0$.

L-68-8513

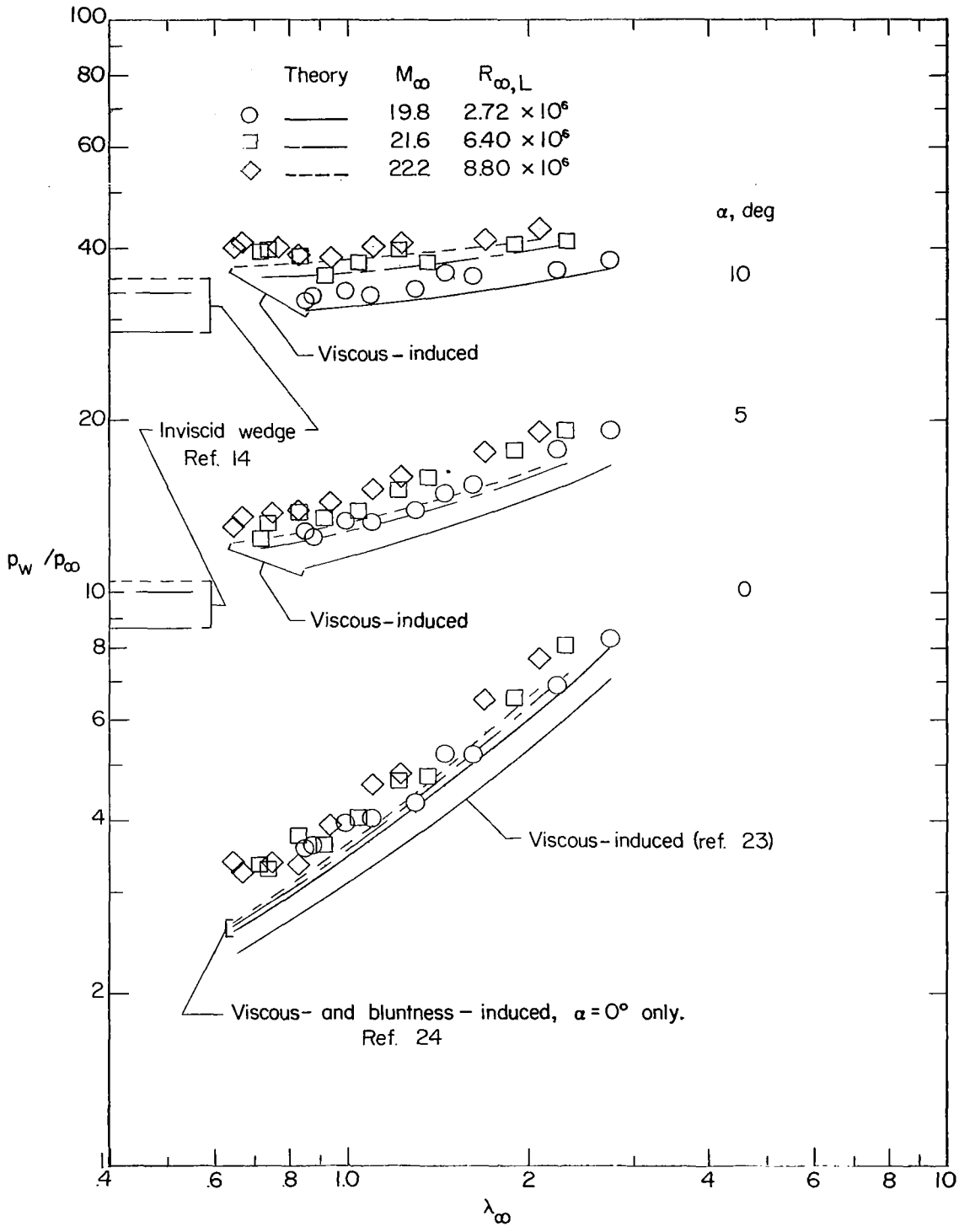

Figure 15.- Flat-plate pressure distributions as a function of the viscous interaction parameter.

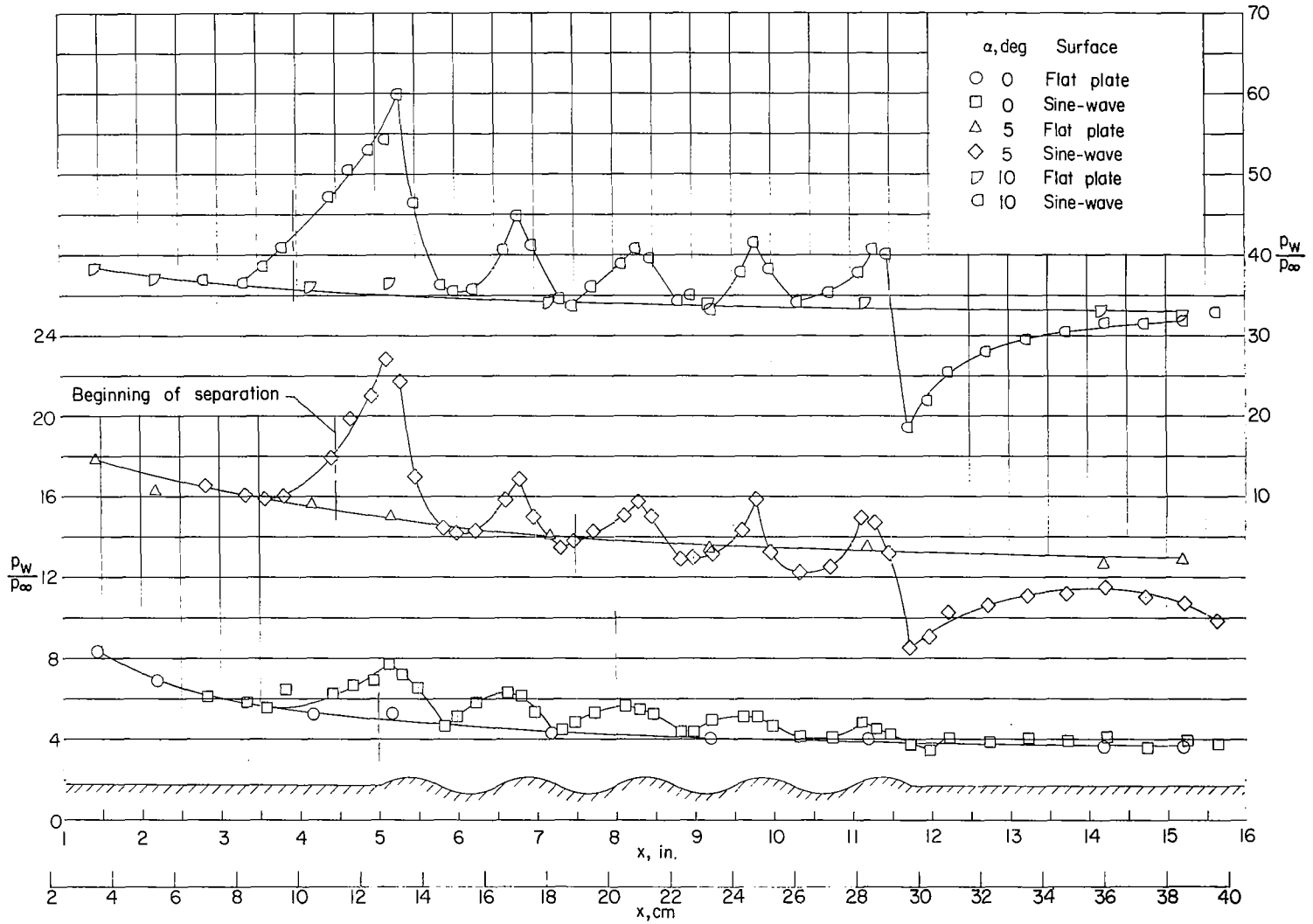

(a) $M_\infty = 19.8$; $R_{\infty,L} = 2.72 \times 10^6$.

Figure 16.- Effect of sine-wave distortion on the surface pressure distribution.

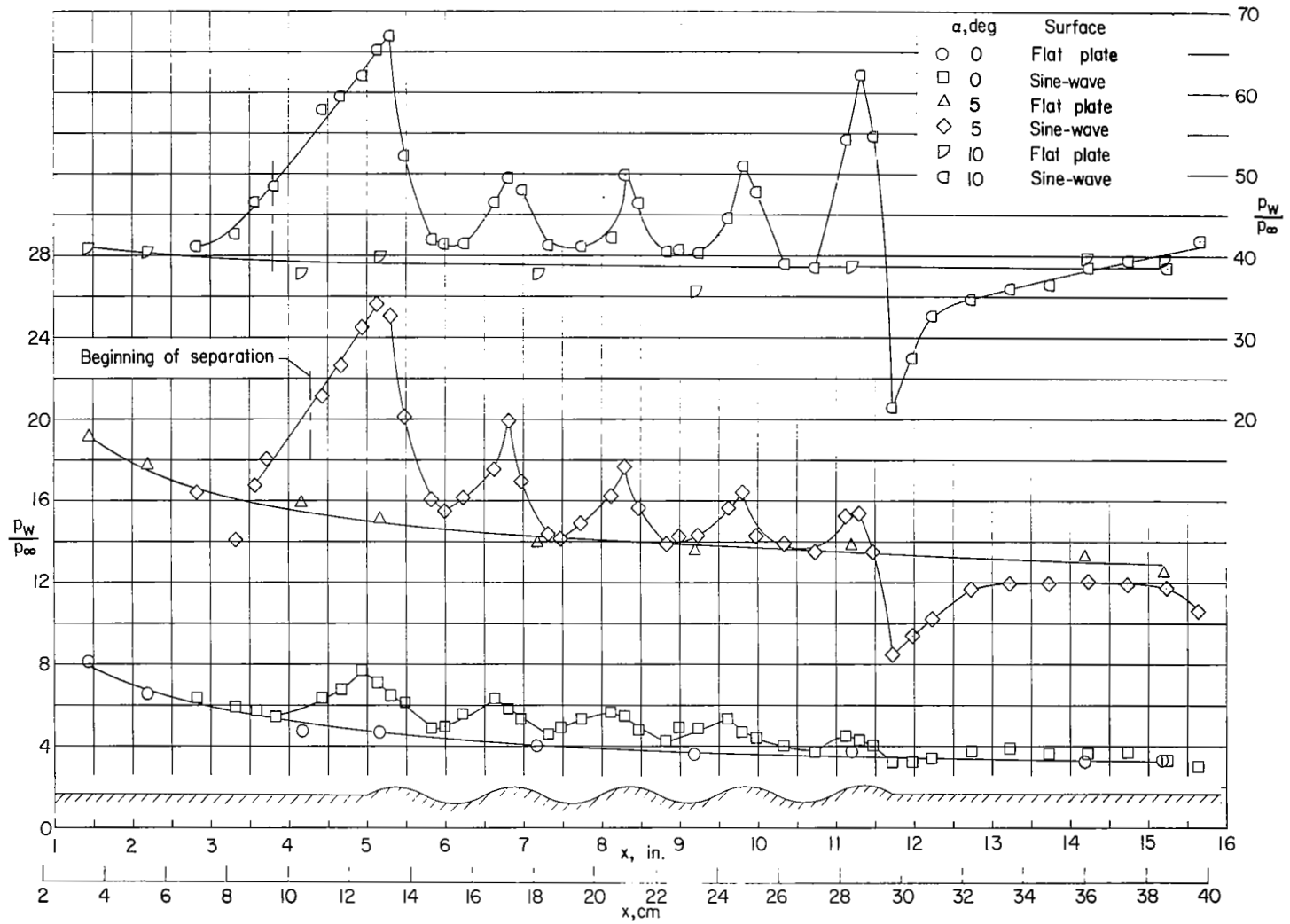

(b) $M_\infty = 21.6$; $R_{\infty,L} = 6.40 \times 10^6$.

Figure 16.- Continued.

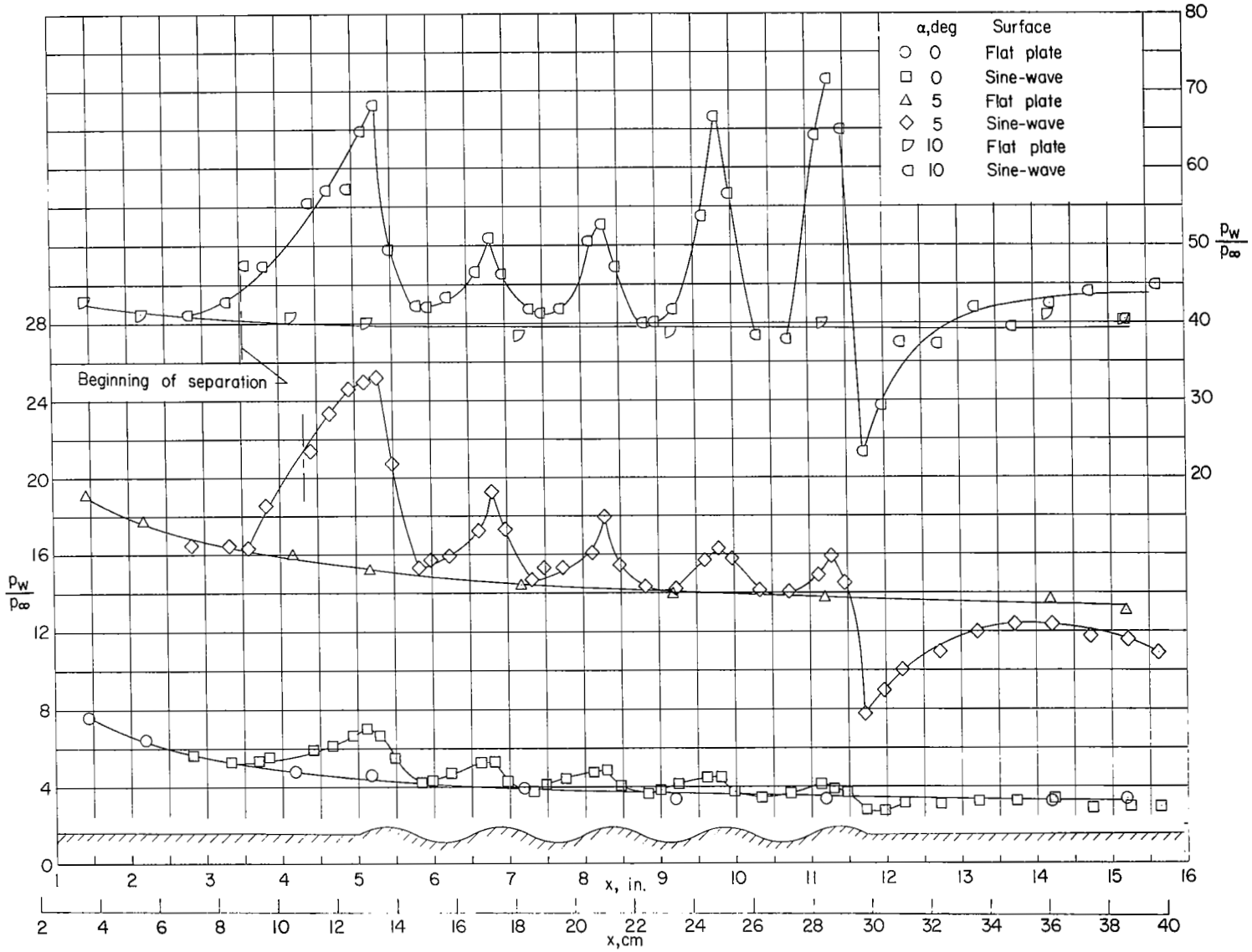

(c) $M_\infty = 22.2$; $R_{\infty,L} = 8.80 \times 10^6$.

Figure 16.- Concluded.

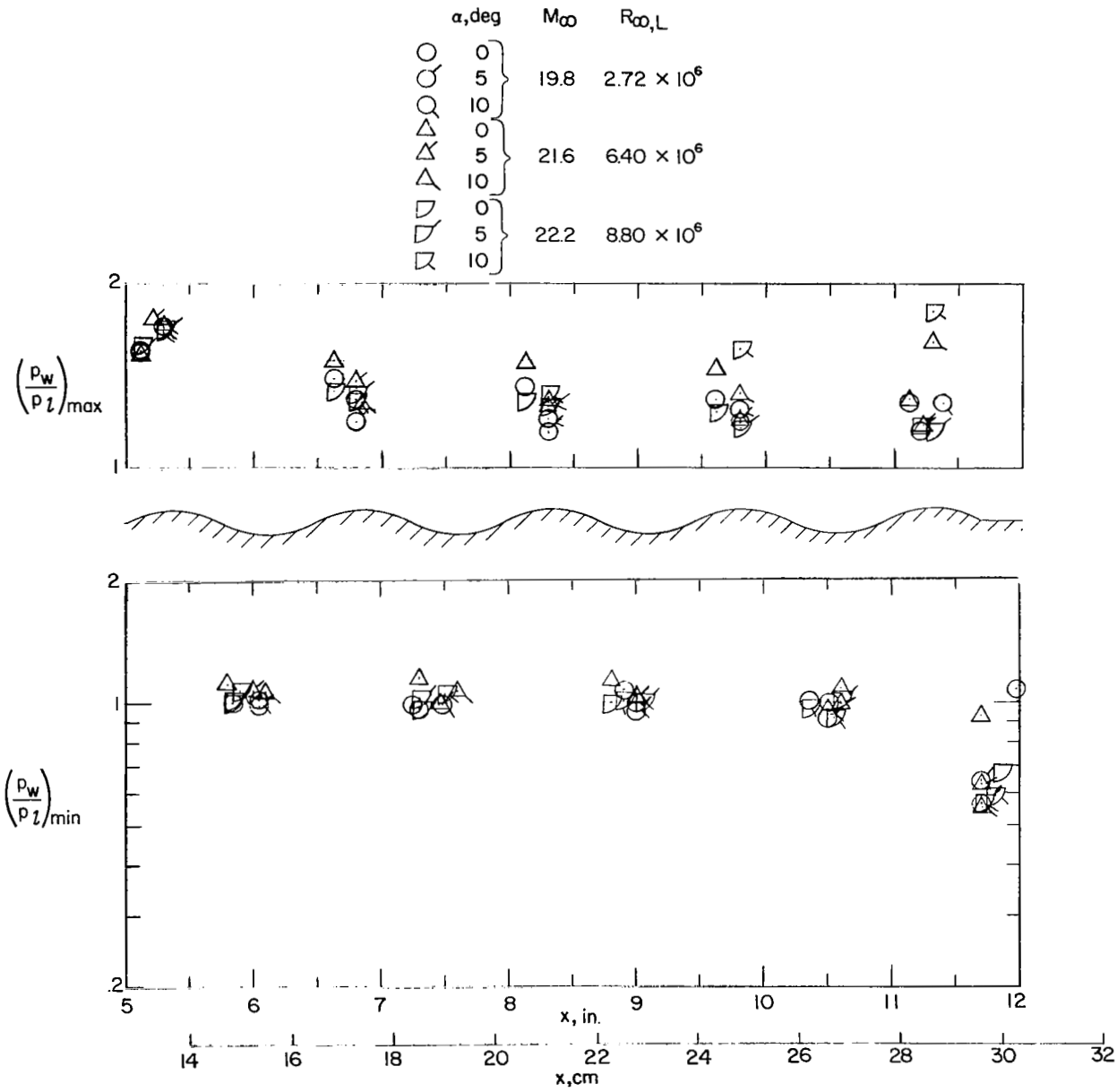

Figure 17.- Maximum and minimum pressures on the distorted surface.

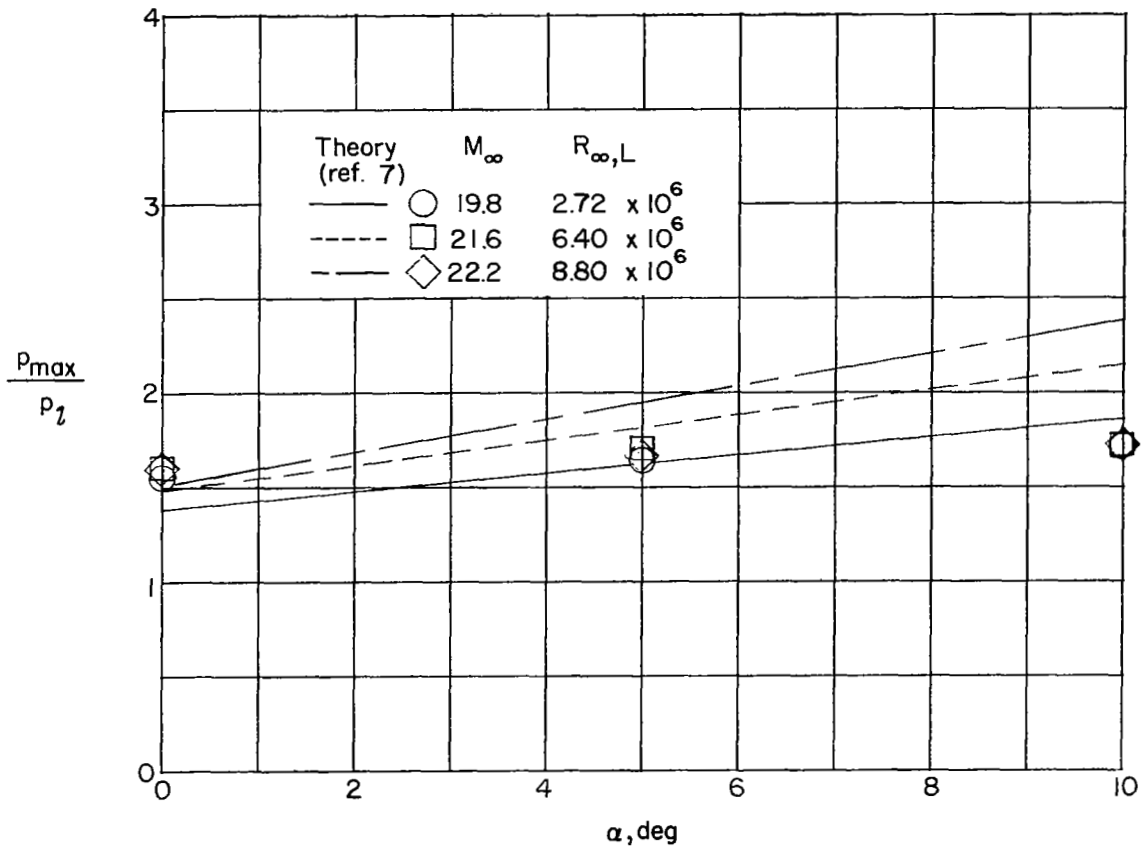

Figure 18.- Comparison of maximum pressure on the first wave with shallow-wave theory.

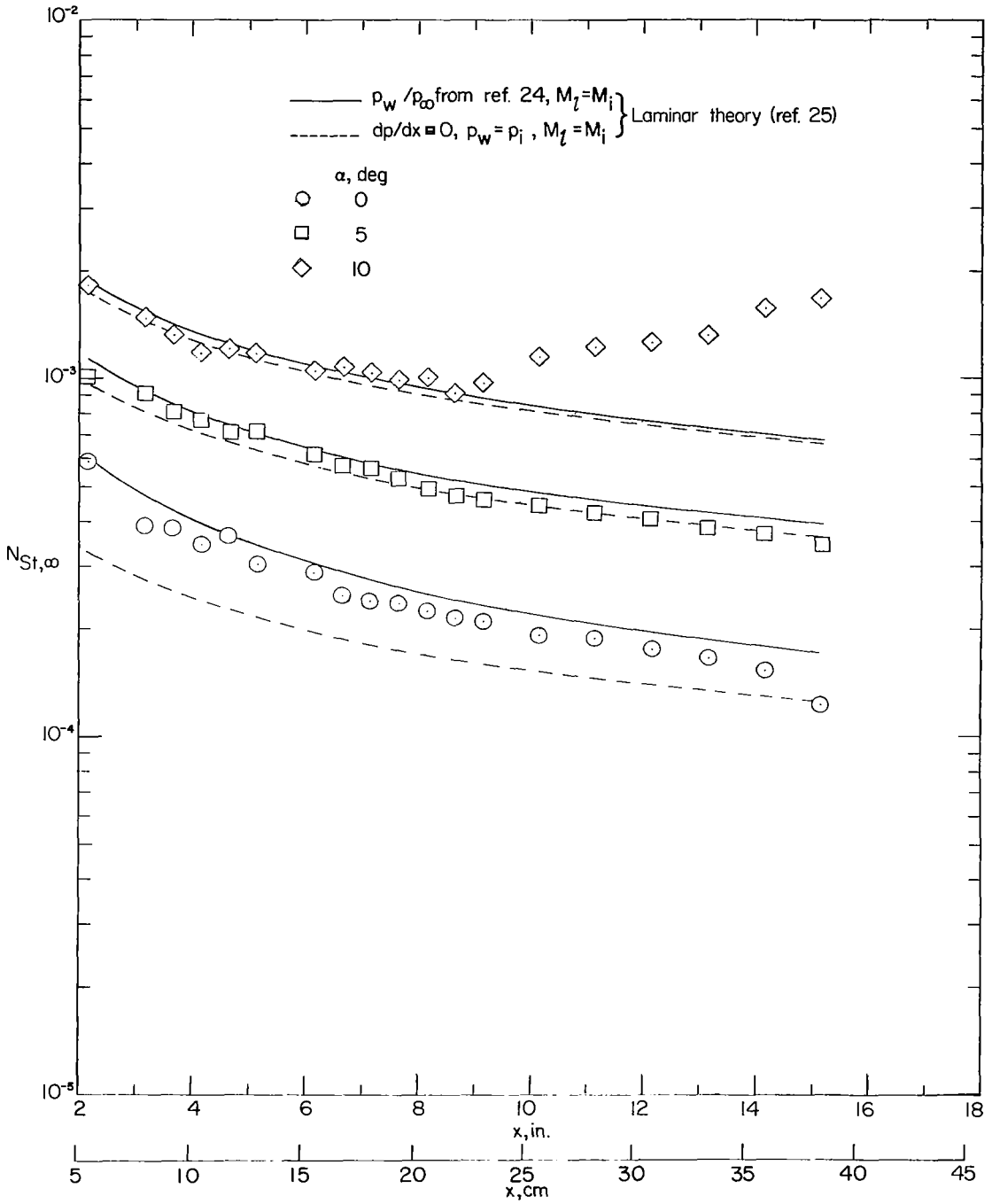

(a) $M_\infty = 19.8$; $R_{\infty,L} = 2.72 \times 10^6$.

Figure 19.- Comparison of heat transfer on the flat surface with laminar theory. $\frac{T_w}{T_t} = 0.62$.

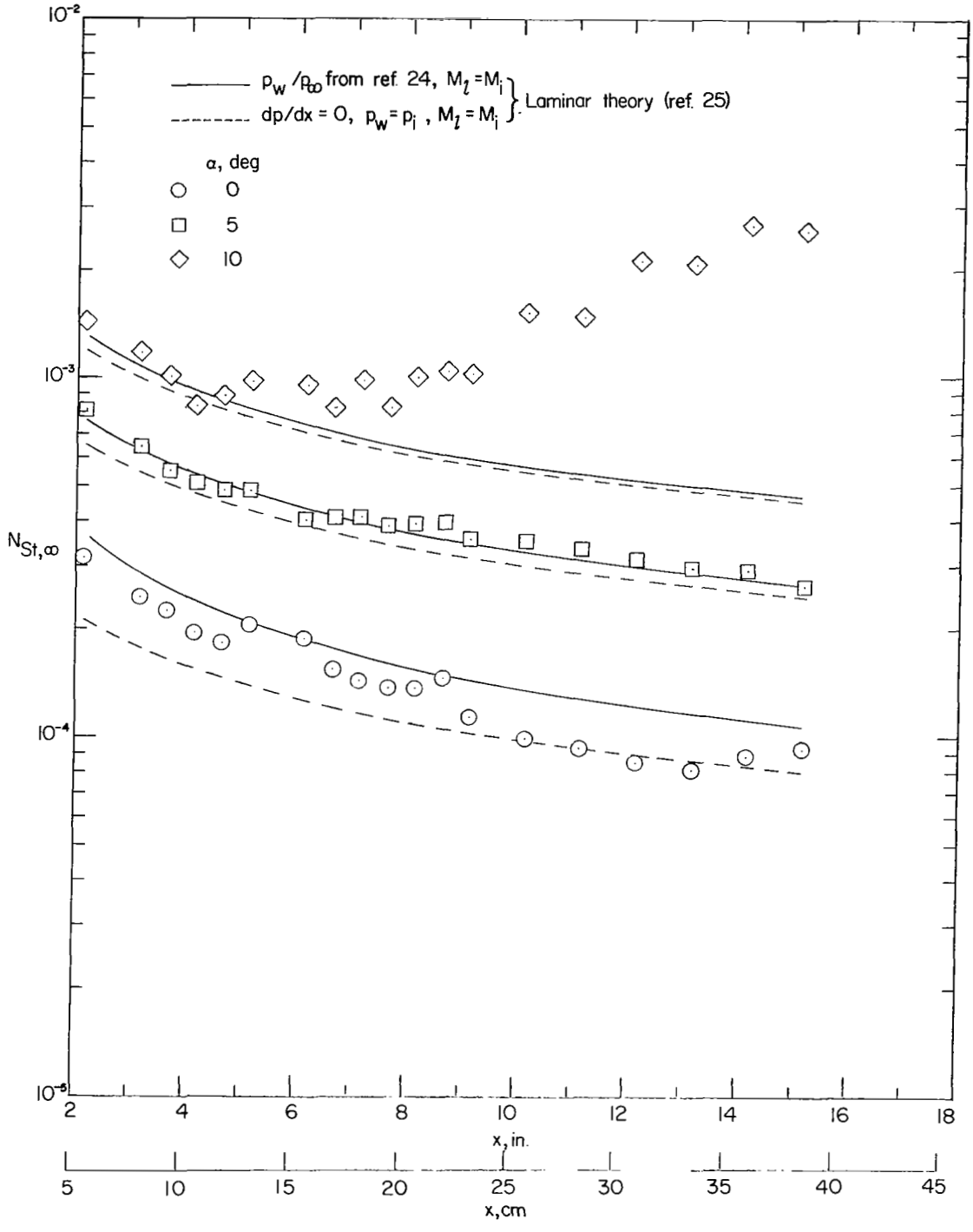

(b) $M_\infty = 21.6$; $R_{\infty,L} = 6.4 \times 10^6$.

Figure 19.- Continued.

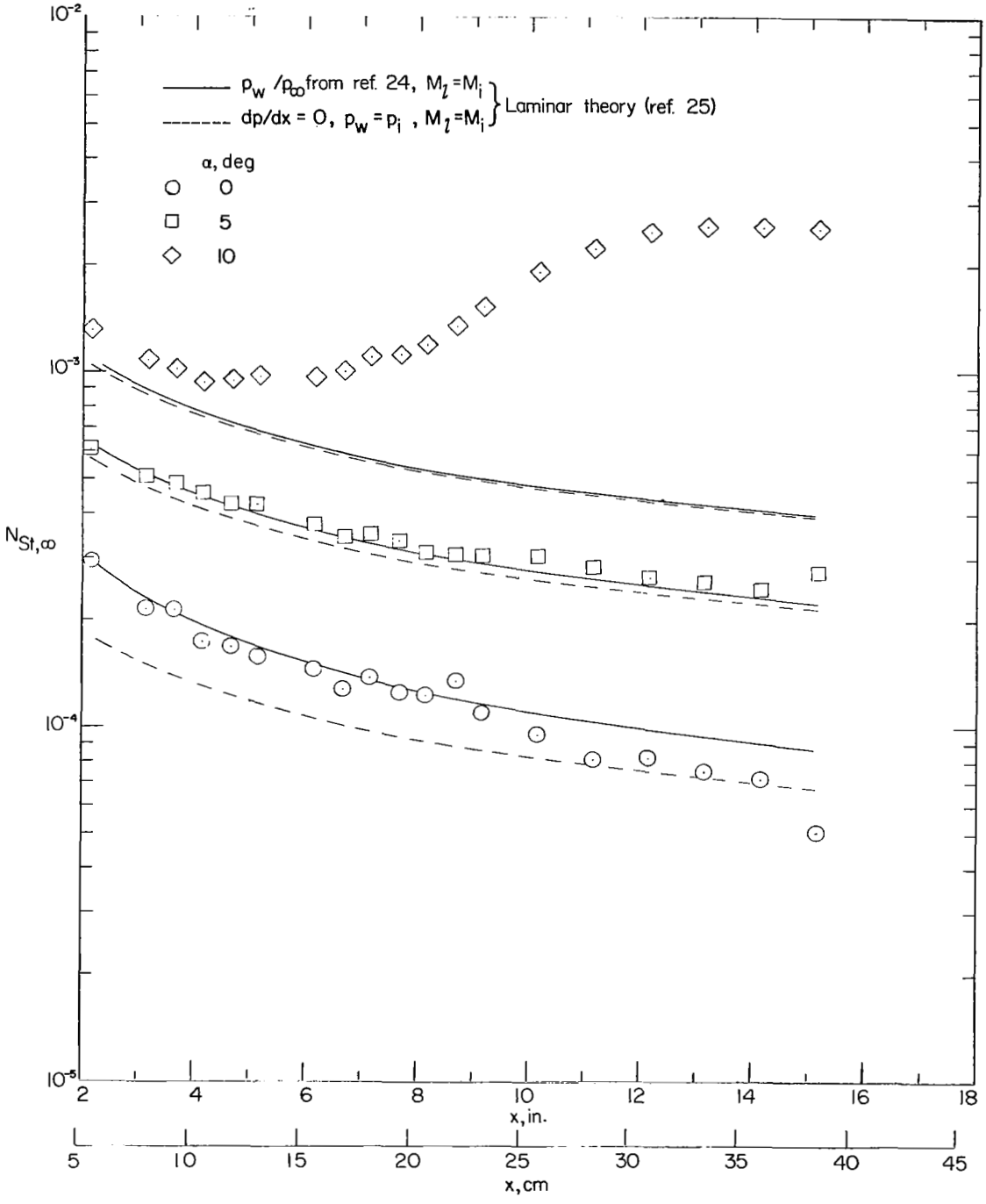

(c) $M_\infty = 22.2$; $R_{\infty,L} = 8.8 \times 10^6$.

Figure 19.- Concluded.

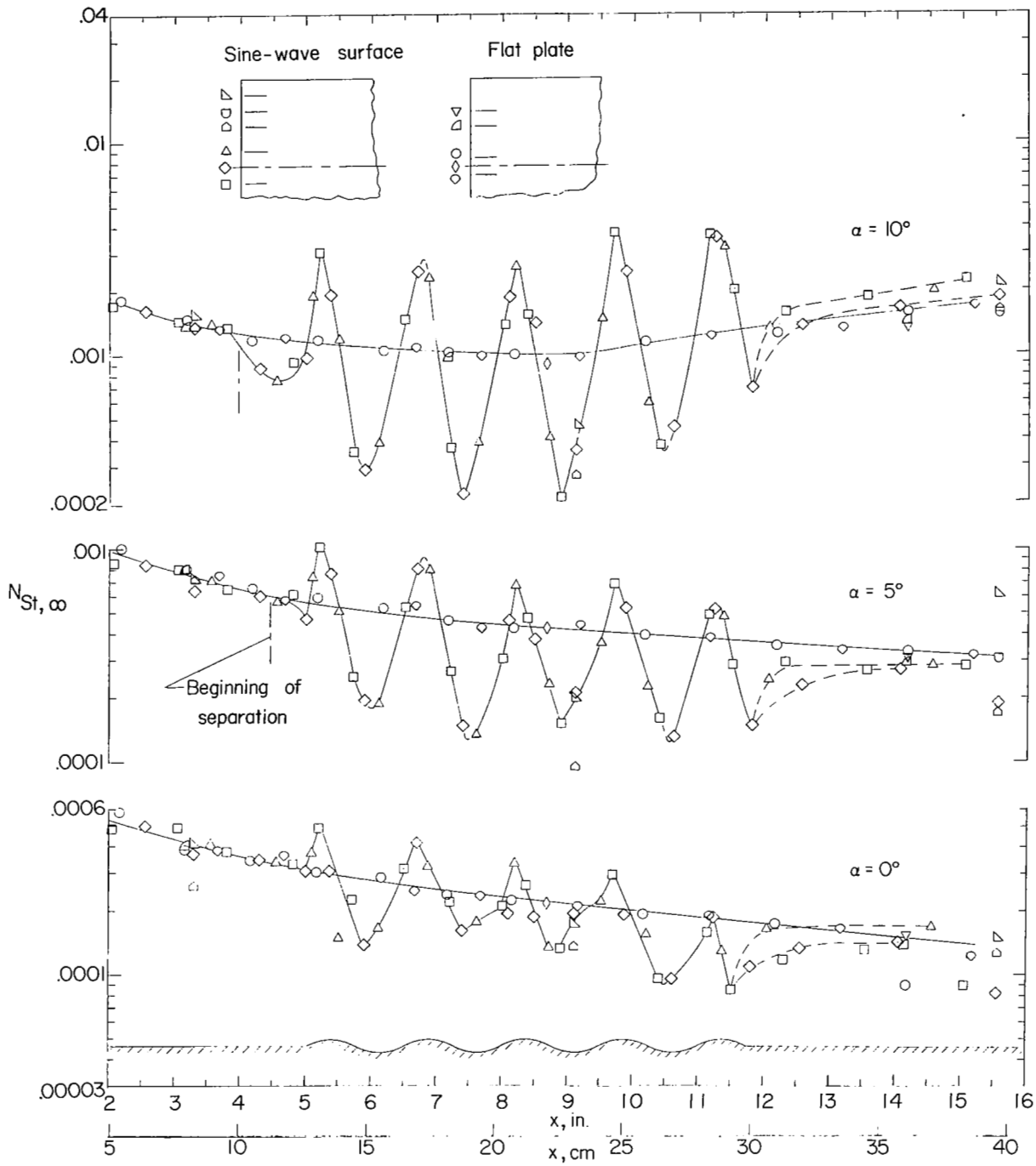

(a) $M_\infty = 19.8$; $R_{\infty,L} = 2.72 \times 10^6$.

Figure 20.- Effect of sine-wave distortion on surface heating. $\frac{T_w}{T_t} = 0.62$.

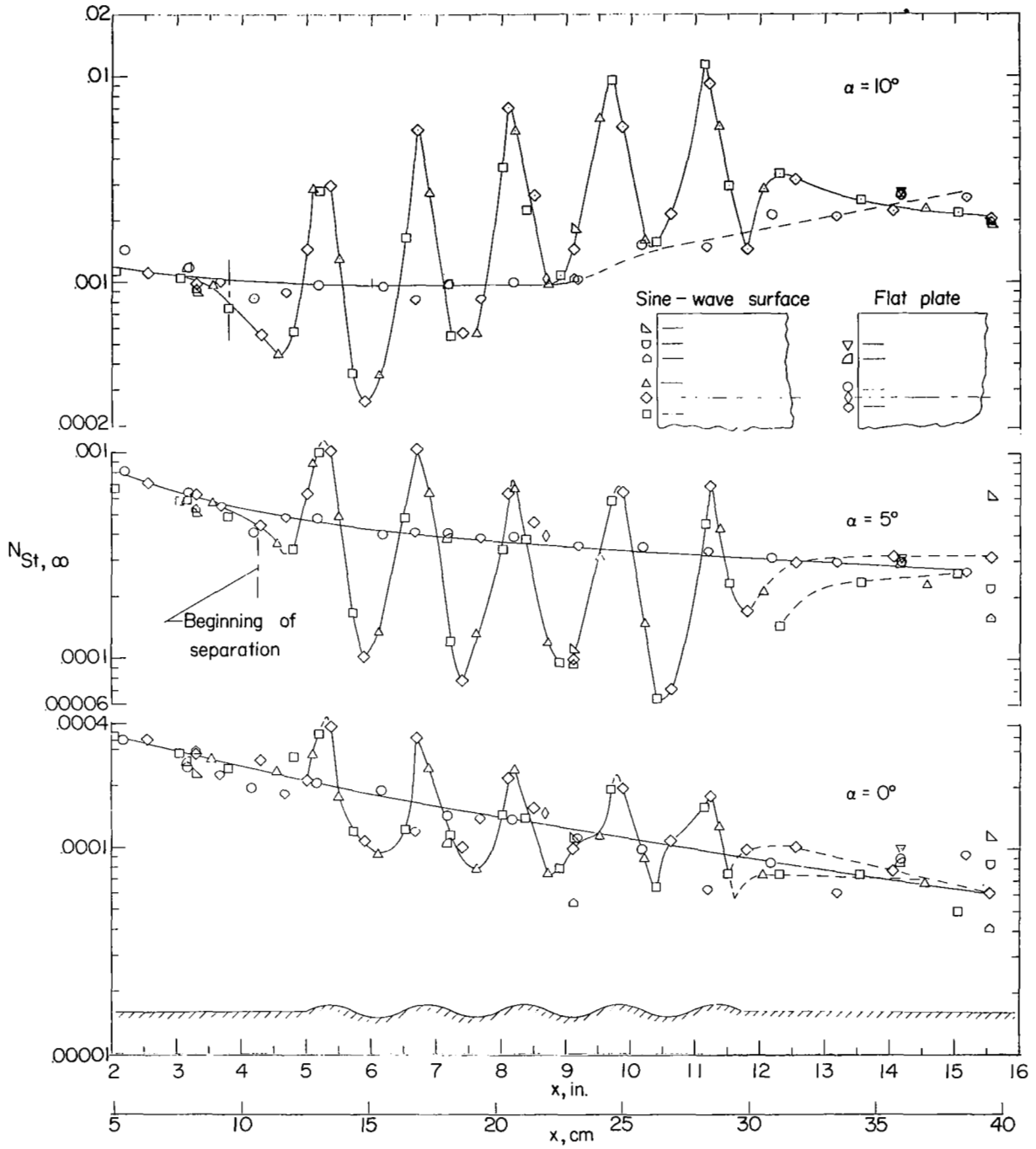

(b) $M_\infty = 21.6$; $R_{\infty, L} = 6.40 \times 10^6$.

Figure 20.- Continued.

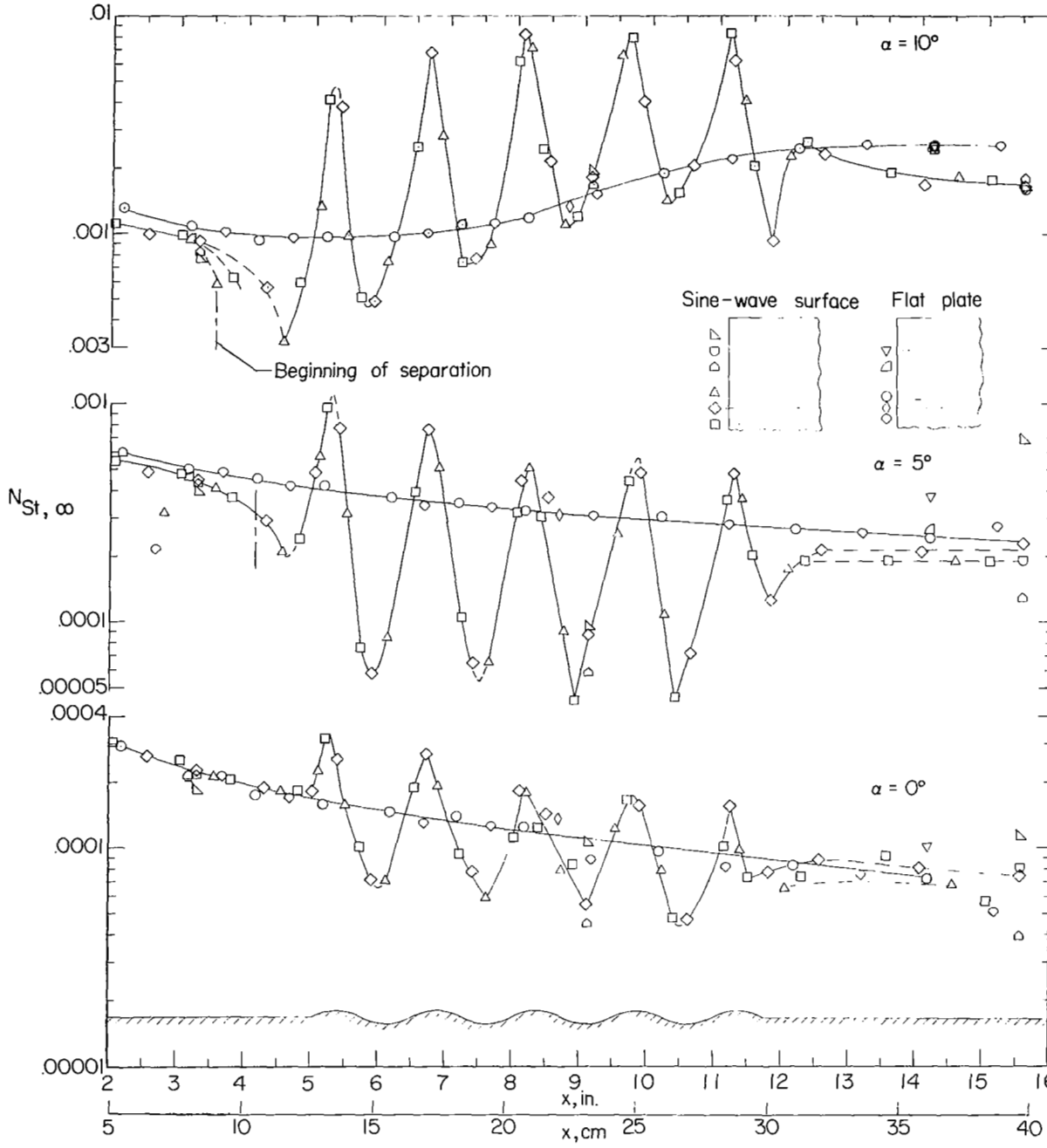

(c) $M_\infty = 22.2$; $R_{\infty,L} = 8.8 \times 10^6$.

Figure 20.- Concluded.

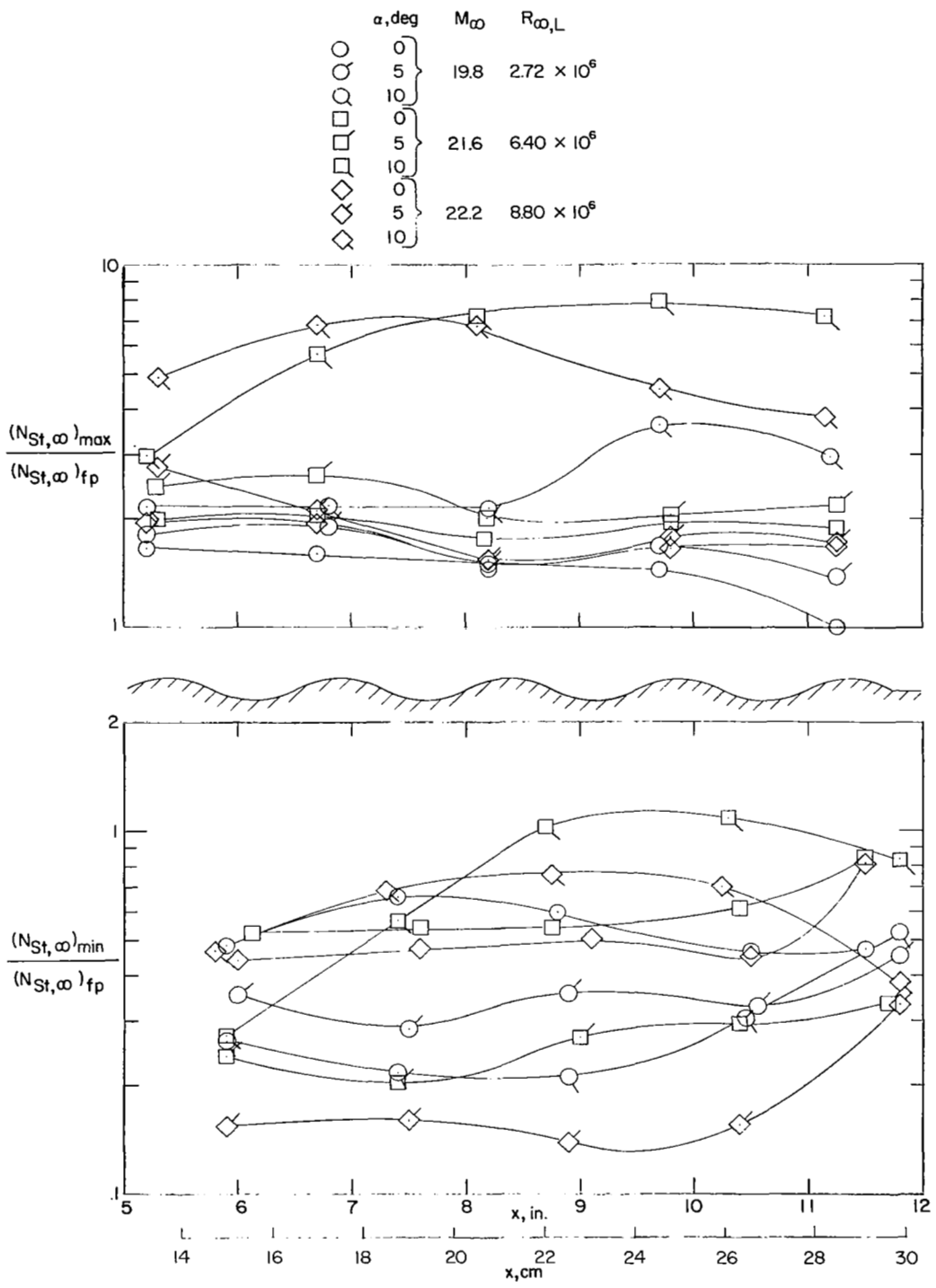

Figure 21.- Maximum and minimum heating on the distorted surface. $\frac{T_w}{T_t} = 0.62$.

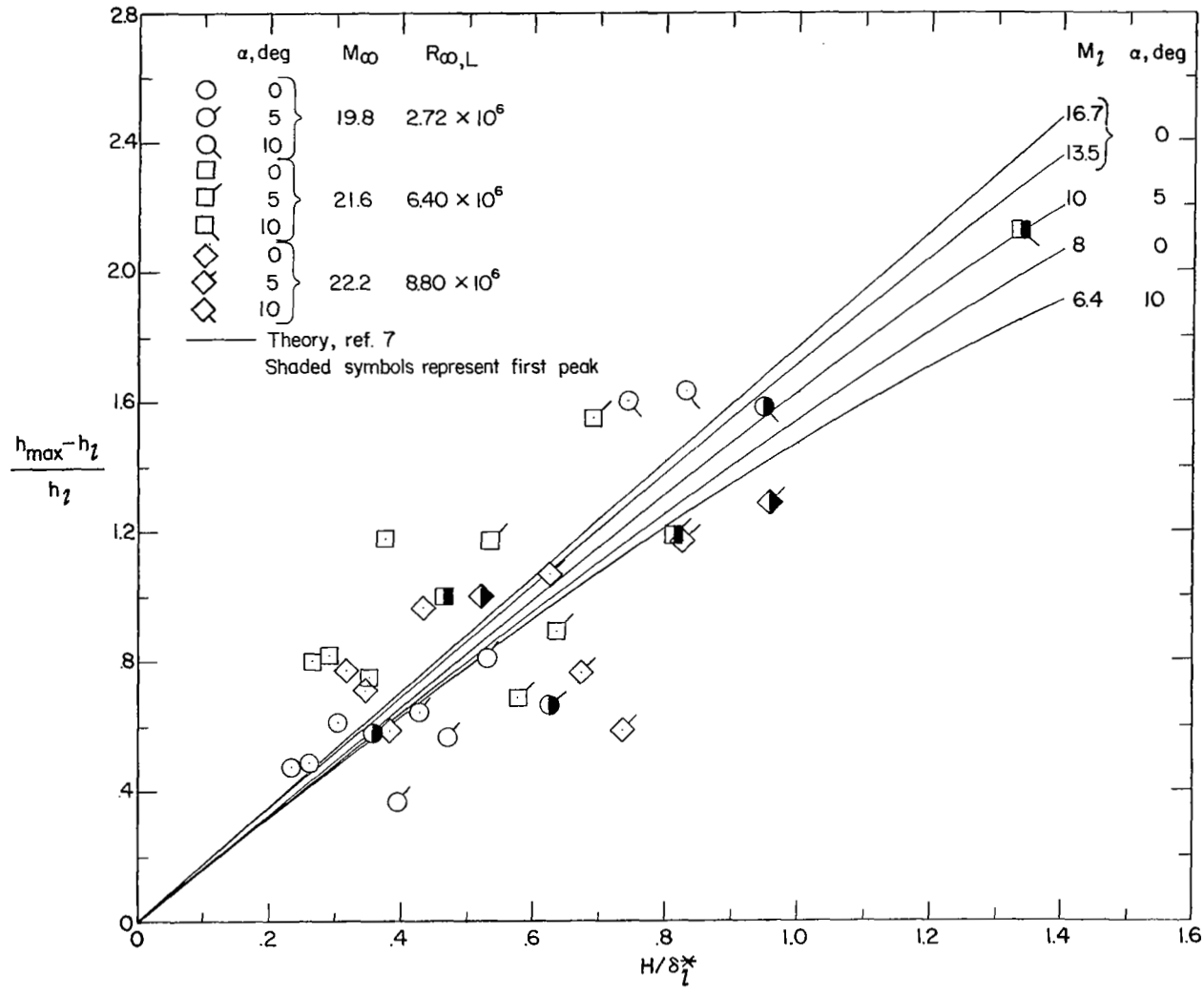

Figure 22.- Comparison of maximum heating with shallow-wave theory. $\frac{T_w}{T_t} = 0.62$.

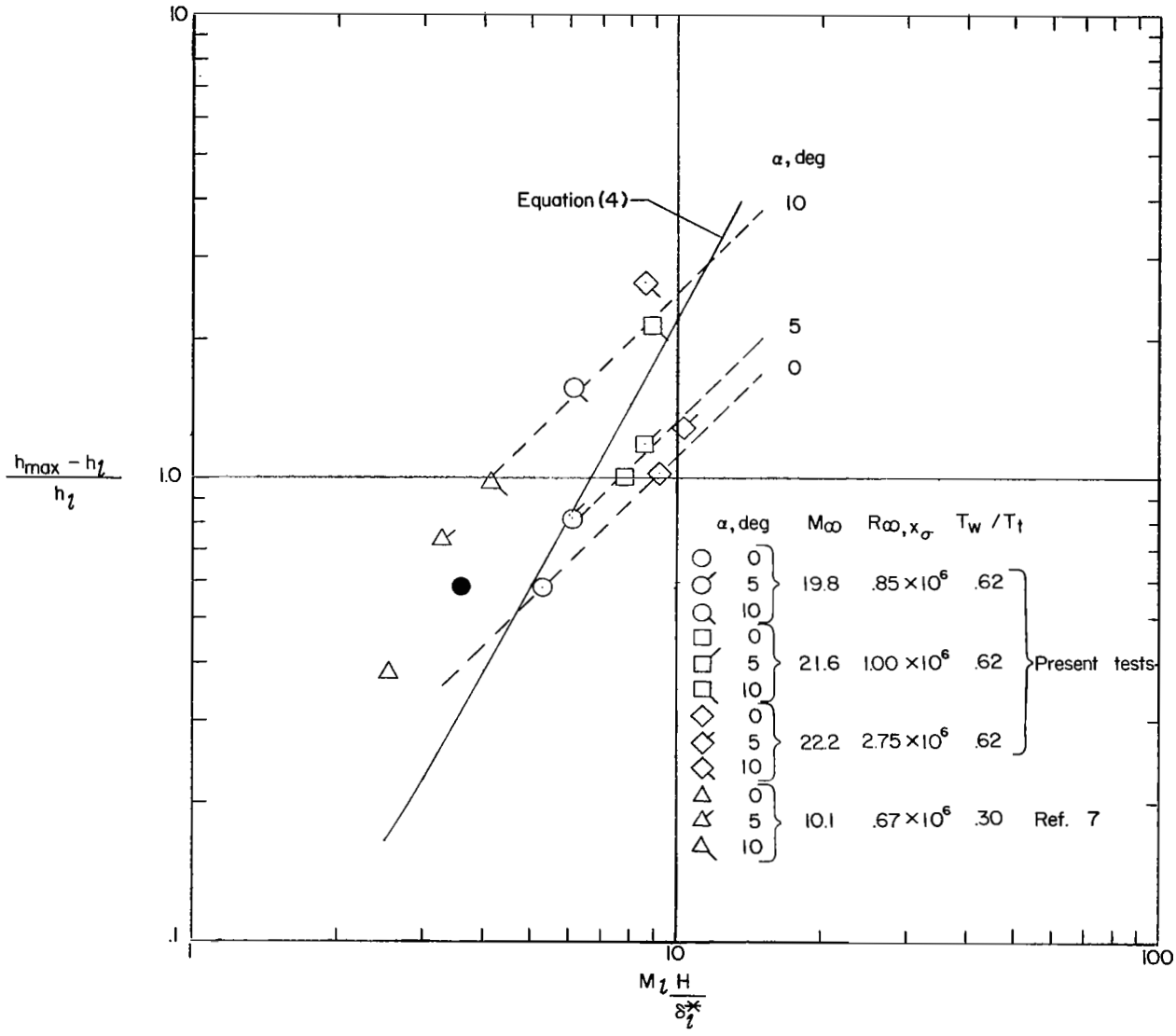

Figure 23.- Maximum heating on the first wave as a function of boundary-layer displacement thickness and local Mach number. Shaded symbol indicates conditions based on boundary-layer survey (M_l = 8).